Refinable tri-variate C^1 splines for box-complexes including irregular points and irregular edges

Jörg Peters[1]Department of Computer & Information Science & Engineering, University of Florida.
(jorg@cise.ufl.edu).

Abstract

C^1 splines over box-complexes generalize C^1 degree 3 (cubic) tensor-product splines. A box-complex is a collection of 3-dimensional boxes forming an unstructured hexahedral mesh that can include irregular points and irregular edges where the layout deviates from the tensor-product grid layout. For example, an edge shared and enclosed by five boxes is irregular. Where the mesh is locally regular, the restriction of the space to each box is a polynomial piece of the C^1 tri-cubic tensor-product spline, by default initialized as a C^2 tri-cubic. Boxes containing irregularities have their polynomials binarily split into 2^3 pieces to isolate the irregularity. The pieces join with matching derivatives. The derivatives are zero at irregularities, but these singularities are removable by a local change of variables. The space consists of 2^3 linearly independent functions per box and is refinable.

Keywords: trivariate C^1 spline; unstructured hex-mesh; singular parameterization; tri-cubic; tensor-product; removable singularity

1. Introduction

The grid points of a regular partition of 3-space into boxes can be interpreted as the control points of a tri-variate tensor-product spline with one polynomial piece per cube. The theory of such splines is well-understood de Boor (1978, 1987). By contrast, for box-complexes where the tensor-grid gives way to an irregular arrangement of boxes including irregular points and irregular edges, there is to date no simple prescription to join the corresponding polynomial pieces with more than C^0 continuity. Efficiently modeling C^1 fields over general box-complexes is of interest in areas ranging from scientific data visualization to solving higher-order differential equations. For example, to visualize a flow computed by the Discontinuous Galerkin approach currently requires substantial post-processing to extract stream lines that the theory predicts to be smooth Walfisch et al. (2009).

Already in two variables – where the box-complex is a quad mesh and the only irregularities are points where more or fewer than four quadrilaterals meet – associating one or more bi-cubic polynomial pieces with each quad and joining them to form a C^1 space is far from trivial. The main options developed over the past 30 years are: geometric continuity (change of variables between pieces) DeRose (1990); Peters (2002); Loop and Schaefer (2008); Karčiauskas and Peters (2016), generalized subdivision Catmull and Clark (1978); Doo and Sabin (1978); Peters and Reif (2008) or introducing singularities into the parameterization Peters (1991a); Neamtu and Pfluger (1994); Reif (1997); Nguyen and Peters (2016). Each option encounters challenges. Geometric continuity requires increased polynomial degree near irregularities and careful book-keeping to adjust reparameterizations under refinement. Subdivision creates an infinite sequence of nested piecewise polynomial rings that complicate engineering analysis, e.g. computing integrals near irregularities. Singular corner parameterizations have shape deficiencies and must ensure that the singularity is locally removable so the resulting space can be certified C^1 despite the vanishing of partial derivatives at irregularities.

In three variables, there are few C^1 constructions for box-complexes with irregularities. The work of the meshing community to generate unstructured hex-meshes Meyers and Tautges (1998); Mitchell (1999); Eppstein (1999); Yamakawa and Shimada (2002); Gregson et al. (2011); Johnen et al. (2017); Owen et al. (2017) and the improved understanding of fields and their singularity graph Nieser et al. (2011); Liu et al. (2018) is not matched by corresponding progress in more flexible spline representations. Trivariate subdivision rules analogous to Catmull-Clark subdivision

Catmull and Clark (1978) have been proposed in MacCracken and Joy (1996) and used in engineering applications in Burkhart et al. (2010) but come without guarantee of smoothness and approximation order. Geometric continuity in three variables, although well-understood in principle, is in practice barely explored: Birner et al. (2018) analyze one pair of face-adjacent boxes.

This paper introduces a trivariate C^1 space with singular parameterization, the third option. Wherever possible, the vertices of the box-complex are interpreted as B-spline coefficients de Boor (1978, 1987). Then, at each irregularity, a well-behaved linear function is determined and composed with a singular local volumetric re-parameterization $\breve{\mathbf{x}}$ that is consistent with the local layout of the box-complex and based on an polytope that is akin to a Voronoi diagram on a sphere enclosing the irregular point. All first derivatives of $\breve{\mathbf{x}}$ are continuous, albeit zero across irregularities. Apart from the irregularities, the Jacobian of $\breve{\mathbf{x}}$ is positive definite. This is a key ingredient to prove that the inverse $\breve{\mathbf{x}}^{-1}$ is well defined and the local expansion of the linear function composed with $\breve{\mathbf{x}}$ can be reparameterized by $\breve{\mathbf{x}}^{-1}$ to remove the singularity. The polynomial pieces of the spline space therefore join not just nominally C^1, but smoothly over the whole box-complex. The spline space has a basis of $2 \times 2 \times 2$ independent functions per hexahedral input box (after a dyadic split of irregular boxes, one for each of the 8 sub-boxes), can reproduce linear functions and is refinable.

Overview. After a brief literature review of bivariate singular constructions, Section 2 defines basic tri-variate concepts, notation and setup. Section 3 initializes a spline space that is C^2 except for zero first derivatives across irregularities. Section 4 defines linear maps at irregularities and Section 5 defines a parameterization that is invertible in a neighborhood of its singularity. Section 6 combines the linear maps and the singular parameterization into an algorithm for constructing a C^1 spline complex. The construction is illustrated both trivariate and the simpler bivariate case. Section 7 establishes C^1 continuity, linear independence of 2^3 B-spline-like functions per box, linear reproduction and refinability of the C^1 spline space. Section 8 briefly discusses alternatives and extensions.

1.1. Bivariate polynomial singular C^1 constructions

To motivate the construction in the remainder of the paper, we first review the bivariate setting. In the bivariate setting, interior mesh points are irregular if they are surrounded, without overlap, by more or fewer than four quads; and quads are irregular if they have one or more irregular points. At irregularities, there is no consistent extension of the individual pieces' parametric derivatives to the whole neighborhood unless their cross-product vanishes (Peters and Reif, 2008, Lemma 3.7). In contrast to geometrically smooth constructions, bivariate, polynomial, parametrically-C^1 constructions therefore need to be singular. Singularly parameterized C^1 surface constructions for irregular quad-layout can be sorted into three categories: subdivision surfaces, where the size of surface rings and hence their parametric derivatives shrink to zero; polar surfaces, where the derivatives along an edge are zero; and singular corner surfaces, where the low-order terms of the Taylor expansion at the corner are zero.

Subdivision surfaces consist of an infinite sequence of nested spline rings. They can be viewed as spline surfaces with a singularity at its central 'extraordinary' point Peters and Reif (2008). There are numerous subdivision variants with the most popular being Catmull-Clark subdivision Catmull and Clark (1978).

Polar surfaces have quad patches with one edge collapsed into the irregular point, called the 'pole', see e.g. Karčiauskas et al. (2006); Karčiauskas and Peters (2007); Myles and Peters (2009, 2011); Shi et al. (2013); Toshniwal et al. (2017a). The patch layout of polar surface parameterizations differs structurally from that of standard subdivision and is most suitable for umbilic points where many pieces meet.

Singular corner constructions collapse the Taylor expansion at the irregular point by setting derivatives to zero Peters (1991a); Pfluger and Neamtu (1993); Neamtu and Pfluger (1994); Reif (1997, 1998); Bohl and Reif (1997); Nguyen and Peters (2016); Karčiauskas and Peters (2017); Toshniwal et al. (2017b). The induced singularity sidesteps the vertex enclosure problem Peters (1991b, 2002), a non-trivial algebraic requirement that arises from forcing the mixed parametric derivatives $\partial_u \partial_v f$ and $\partial_v \partial_u f$ to agree. Accordingly, 'Parametrizing singularly to enclose vertices by a smooth parametric surface' Peters (1991a) sets the mixed derivatives to zero. Reif (1997) proved that, if higher partial derivatives are suitably constrained, such singularities are locally removable. That is, the parametric singularity need not correspond to a geometric singularity. In contrast to subdivision, a finite number of polynomial pieces with singular parameterization are straightforward to include into existing CAD modeling environments. However, the resulting C^1 surfaces typically have poor shape when used for free-form design. A recent variant, proposed in Karčiauskas and Peters (2017), removes visible shape defects but at the cost of increased polynomial degree and overall complexity.

Gregory (1974); Warren (1992) impose *rational* singularities to avoid having to enforce $\partial_u \partial_v f = \partial_v \partial_u f$. The cost is increased complexity, rational representation and higher degree than singular corner constructions.

After a gap of two decades, Nguyen and Peters (2016) renewed interest in the singular constructions by focusing on engineering analysis and functions on irregular bivariate 2-manifolds. Combining the singular splines with PHT-splines Kang et al. (2015), (a.k.a. bi-cubic finite elements with hanging nodes in the finite element literature) yields a bi-cubic C^1 space with adaptive refinability. Nguyen and Peters (2016) demonstrate the space's effectiveness for modeling and solving thin plate challenge problems of the finite element obstacle course, such as the 'octant of a sphere' and the 'Scordelis-Lo roof'. Wei et al. (2018) adapts the bivariate approach to tri-cubic splines but with only C^0 continuity across extraordinary edges and vertices.

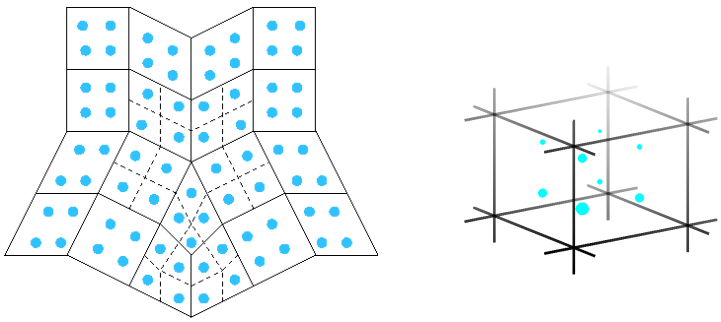

(a) bivariate box-complex (b) trivariate $\mathbf{c}^s_\alpha$

Figure 1: Bivariate box-complex (a) and one trivariate box (b). For each box H^s, blue bullets mark 2^m control points $\mathfrak{c}^s_\alpha := (\mathbf{c}^s_\alpha, y^s_\alpha)$, consisting of control abscissae $\mathbf{c}^s_\alpha$ and associated data y^s_α, enumerated by the multi-index α. The control points $\mathfrak{c}^s_\alpha$ scale the basis functions f^s_α of a piecewise polynomial $\sum_{s,\alpha} \mathfrak{c}^s_\alpha f^s_\alpha$. (a) Dashed lines partition polynomial pieces near irregularities of valence $n = 3$ and 5. Each regular, unpartitioned quad is associated with four control points and one bi-cubic polynomial. Each irregular quad is equally associated with four control points but four polynomial pieces, one per sub-box (dashed quad). (b) The 8 control abscissae $\mathbf{c}^s_\alpha$, $1 \le \alpha_i \le 2$ of a tri-variate box.

Like its predecessors, the construction of Nguyen and Peters (2016) collapses the first-order jet and then projects the lowest-order non-zero expansion terms at the irregular point into a fixed plane. Unlike its predecessors, it associates with each irregular quad not just one but four polynomial pieces (see Fig. 1a). This 'splitting' localizes the operations that make the space C^1 and so allows irregular points in close proximity. Moreover, splitting yields linearly independent functions, one per control point, and it simplifies the space's use for computations: every input quad, regular or irregular, now contributes exactly 2×2 degrees of freedom, i.e. weights that scale linearly independent functions.

The construction of this paper, too, leverages splitting to isolate irregularities. The resulting generalized spline basis will consist of 2^3 functions and their control points for each input box, see Fig. 1b. The construction differs from its predecessors in that, instead of projecting, C^1 continuity is ensured by explicitly building the spline as a composition of a regular linear map with a singularly parameterized expansion that has a local inverse.

2. Notation and Indexing

In the following, we denote the number of variables by m to avoid any confusion with the polynomial degree 3 or an edge valence that might be $n_e = 3$. Except for some illustrations that explicitly specify $m = 2$, by default throughout $m := 3$.

Box-complex. Analogous to a simplicial complex, a *box-complex* in $\mathbb{R}^m$ is a collection of d-dimensional boxes, $0 \le d \le m$, called d-boxes. Boxes of any dimension overlap only in complete lower-dimensional d-boxes. A 0-box is a vertex, a 1-box an edge, a 2-box a quadrilateral and a 3-box is a quadrilateral-faced hexahedron. A box without prefix is a 3-box. Until the discussion of box faces on the global boundary in Section 8, we focus exclusively on interior d-boxes, i.e. boxes fully surrounded by boxes.

Irregularities. For $d < m$, an interior d-box is *regular* if it is completely surrounded by 2^{m-d} boxes and, for $m > \bar{d} > d$, all incident $\bar{d}$-boxes are regular. For example, for a vertex to be regular, all edges incident to it must be

regular. For $m = 3$, a regular vertex ($d = 0$) is surrounded by 8 boxes, a regular edge ($d = 1$) by 4 boxes and a regular quadrilateral face ($d = 2$) by 2 boxes. Interior faces are always regular since they are shared by exactly 2^1 boxes. To simplify the treatment of essentially bi-variate irregularities, we define a 0-box to be *semi-regular* (blue point in Fig. 2b) if (i) it is shared by two edges that are each surrounded by $n_e \neq 4$ boxes and (ii) it is fully surrounded by $2n_e$ boxes. An edge connecting two semi-regular points is a *semi-regular edge*. A 1-box that is not a semi-regular edge but is surrounded by $n_e \neq 4$ boxes is called an *irregular edge*. A point that is neither regular nor semi-regular is an *irregular point*. Boxes with one or more irregular points will be evenly split into 2^m sub-boxes so that the sub-boxes contain at most one irregular point each.

A box is regular if all its vertices are regular. Otherwise the box is irregular.

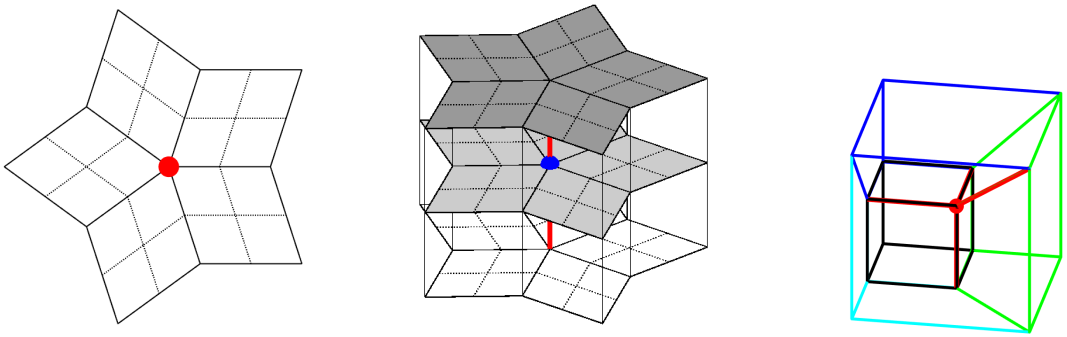

(a) $m = 2, d = 0$ (b) $m = 3, d = 1$ (c) $m = 3, d = 0, n = 4$

Figure 2: Irregularities of (a) irregular point: dimension $d = 0$ in $\mathbb{R}^2$ and (b) irregular edge: dimension $d = 1$ in $\mathbb{R}^3$. The blue point • in (b) is semi-regular due to the tensored structure in the axis direction. (c) Four boxes in $\mathbb{R}^3$: one irregular point of valence $n = 4$ and four irregular edges of valence $n_1 = 3$.

Example: Fig. 2a shows five planar quadrilaterals surrounding a central irregular point without overlap or gap. When the quadrilaterals are extruded to form five pairwise-connected boxes, two layers of five boxes share a semi-regular point (blue in Fig. 2b). If the top and bottom 5-valent point are not semi-regular, the two edges forming the axis are irregular. If the stacked configuration continues to a third layer of five boxes, the middle edge is a semi-regular edge. The dotted lines in Fig. 2b hint at the partition of the C^1 spline construction into polynomial pieces near edge irregularities. Fig. 2c illustrates an irregular point enclosed by four boxes. ◇

Polynomial pieces, corner and inner coefficients. We abbreviate

$$e_j(l) := \begin{cases} 1, & \text{if } l = j, \\ 0, & \text{else} \end{cases} \qquad e_0 := \mathbf{0} := (0, \ldots, 0),$$

where the size of the vectors is determined by context. By default $e_j \in \mathbb{N}_0^m$. Each regular box is associated with one polynomial piece. Each irregular box is associated with 2^m polynomial pieces. Each piece $\mathbf{x}$ will be represented in m-variate *tensor-product* Bernstein-Bézier (BB) form of polynomial degree 3 in each variable (see Farin (2002) or Prautzsch et al. (2002)):

$$\mathbf{x}(\mathbf{u}) := \sum_{\alpha:\ 0 \le \alpha_i \le 3} \mathbf{x}_\alpha \prod_{i=1}^{m} B^3_{\alpha_i}(u_i), \quad \mathbf{u} \in [0..1]^m, \quad \alpha := (\alpha_1, \ldots, \alpha_m),$$

where $B^3_k(t) := \binom{3}{k}(1-t)^{3-k}t^k$ are the Bernstein-Bézier (BB) polynomials of degree 3 and the row vectors $\mathbf{x}_\alpha \in \mathbb{R}^m$ are the BB-coefficients. Specifically, for $m = 3$, $\alpha := (i, j, k)$, $\mathbf{u} := (u, v, w)$,

$$\mathbf{x}(u, v, w) := \sum_{i=0}^{3}\sum_{j=0}^{3}\sum_{k=0}^{3} \mathbf{x}_{ijk} B^3_i(u) B^3_j(v) B^3_k(w). \tag{1}$$

De Casteljau's algorithm can be used to evaluate the BB-form (1) and to re-express a polynomial on a subdomain of $[0..1]^m$. Connecting $\mathbf{x}_\alpha$ to $\mathbf{x}_{\alpha+e_j}$ whenever $\mathbf{x}_{\alpha+e_j}$ is well-defined, yields a mesh called the *BB-net* (see e.g. Fig. 4a). The BB-coefficients are *associated* with d-boxes. Setting $\alpha_i := 0$ (or, symmetrically $\alpha_i := 3$) for exactly one $i \in \{1,2,3\}$ leaves 4×4 BB-coefficients that define $\mathbf{x}$ restricted to a quad face of the domain cube. Setting $\alpha_i := \alpha_j := 0$ for $i \neq j$ yields the BB-coefficients of a polynomial restricted to an edge E_k in the direction e_k, $i \neq k \neq j$. The 2^m BB-coefficients $\mathbf{x}_\alpha$ with $\alpha \in \{0,3\}^m$ are called *corner BB-coefficients* since they are the values of $\mathbf{x}$ in the domain corners $\mathbf{u} \in \{0,1\}^m$. By default we arrange the domain axes so that the irregular point under consideration corresponds to $\mathbf{x_0}$ and an irregular edge to $\mathbf{x}_{\gamma,0,0}$. The 2^d BB-coefficients $\mathbf{x}_{\gamma,\alpha}$, with $0 < \alpha_i < 3$, $1 \leq i \leq d$ and $\gamma_j \in \{0,3\}$ are called *inner with respect to a d-box* (see e.g. Fig. 5b). For example $\mathbf{x}_{001}$ and $\mathbf{x}_{002}$ are inner with respect to the 1-box (edge) associated with the univariate polynomial $\sum_{k=0}^{3} \mathbf{x}_{00k} B_k^3(w)$.

Let H^s, $s = 1, \ldots, n$, be the n boxes joining at and surrounding an irregularity. Then their BB-coefficients are labeled $\mathbf{x}_\alpha^s$.

BB-coefficients $\breve{\mathbf{x}}_\alpha^s$, with indices α in a set G defined below, define the Taylor expansion $\breve{\mathbf{x}}$ of a tri-cubic at $(0,0,0)$ to at most second-order in each variable.

BB-net neighborhoods and their index sets. To render the description of the construction more intuitive, we define index sets and corresponding groups of BB-coefficients, called neighborhoods (see also Fig. 3 and Fig. 4). The *tangent-neighborhood* of a point $\mathbf{x_0}$, surrounded by boxes H^s, $s = 1, \ldots, n$, is

$$\breve{\mathbf{x}}_T := \{\breve{\mathbf{x}}_\alpha^s : \alpha \in T, s = 1, \ldots, n\},\ T := \{e_j \in \mathbb{N}_0^m :\ j = 0, \ldots, m\}.$$

The *bivariate* γ tangent-neighborhoods of edge E_i surrounded by boxes H^s, $s = 1, \ldots, n_i$ is

$$\breve{\mathbf{x}}_{T_{\gamma,i}} := \{\breve{\mathbf{x}}_\alpha^s : \alpha \in T_{\gamma,i},\ s = 1, \ldots, n_i\},\ T_{\gamma,i} := \{\gamma e_i + e_j, j \in \{0, \ldots, m\}, j \neq i, \}.$$

The *1-neighborhoods* are

$$\breve{\mathbf{x}}_A := \{\breve{\mathbf{x}}_\alpha^s : \alpha \in A, s = 1, \ldots, n\},\ A := \{\alpha :\ 0 \leq \alpha_j \leq 1,\ \text{for } j = 1, \ldots, m\},$$
$$\breve{\mathbf{x}}_{A_{\gamma,i}} := \{\breve{\mathbf{x}}_\alpha^s : \alpha \in A_{\gamma,i}, s = 1, \ldots, n_i\},\ A_{\gamma,i} := \{\alpha :\ \alpha_i = \gamma, 0 \leq \alpha_j \leq 1,\ \text{for } j \in \{1, \ldots, m\}, j \neq i\}.$$

For edges E_i, $i = 1, 2, 3$, emanating from $\mathbf{x_0}$ and boxes H^s, $s = 1, \ldots, n$, the *projection neighborhood* consists of

$$\breve{\mathbf{x}}_\Gamma := \{\breve{\mathbf{x}}_\alpha^s : \alpha \in \Gamma, s = 1, \ldots, n\}, \quad \Gamma := \Big\{e_i + \sum_{l=1}^{m} e_l + (e_j \text{ if } E_i \text{ is irregular}) : \quad i, j = 1, \ldots, m, j \neq i\Big\}.$$

That is, for

$$m = 2, \quad \Gamma := \{2e_i + e_j : i = 1, 2, \{e_i, e_j\} = \{1, 2\}\};$$
$$m = 3, \quad \Gamma := \Big\{ \begin{cases} 2e_i + e_j + e_k & \text{if } E_i \text{ is regular;} \\ 2e_i + 2e_j + e_k \text{ and } 2e_i + e_j + 2e_k & \text{if } E_i \text{ is irregular;} \end{cases}, i = 1, 2, 3, \{e_i, e_j, e_k\} = \{e_1, e_2, e_3\}\Big\}.$$

The index set Γ does not include (222), or indices of BB-coefficients that will be determined as an average of their index-wise nearest neighbors. (Two BB-coefficients $\mathbf{x}_\alpha^s$ and $\mathbf{x}_\beta^s$ are *index-wise nearest* if there is no $\mathbf{x}_\gamma^s$ with $\|\alpha - \gamma\|_1 < \|\alpha - \beta\|_1$ in the ℓ_1-norm). The union of neighborhoods is denoted

$$G := A \cup \Gamma \cup_{i=1}^{m} A_{2,i}.$$

Example: For $m = 2$, the only irregularities are points,

$$A = \{(0,0), (1,0), (0,1), (1,1)\}, A_{2,1} = \{(2,0), (2,1)\} \text{ and } \Gamma = \{(2,1), (1,2)\},$$

see Fig. 3. The algorithm in Nguyen and Peters (2016) can be reformulated in terms of A and Γ. $\diamond$

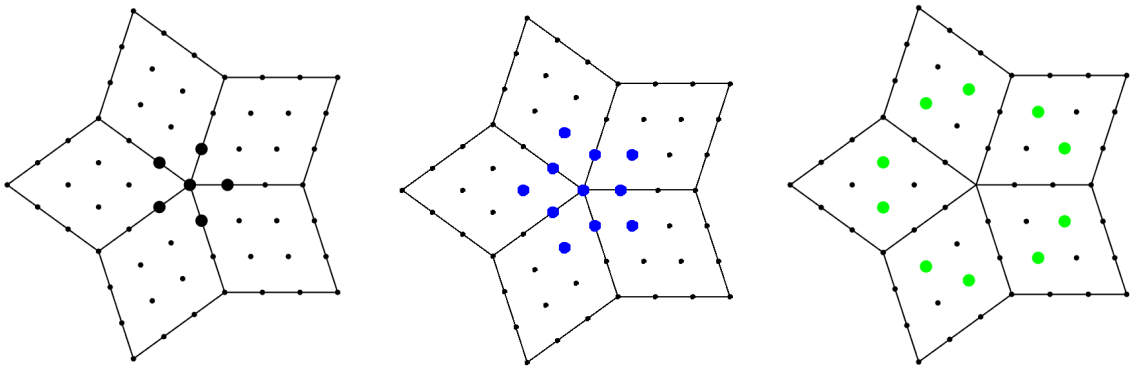

(a) $\breve{\mathbf{x}}_T$ (b) $\breve{\mathbf{x}}_A$ (c) $\breve{\mathbf{x}}_\Gamma$

Figure 3: $m = 2$: BB-coefficients of a local box-complex for with neighborhoods $\breve{\mathbf{x}}_T$, $\breve{\mathbf{x}}_A$ and $\breve{\mathbf{x}}_\Gamma$.

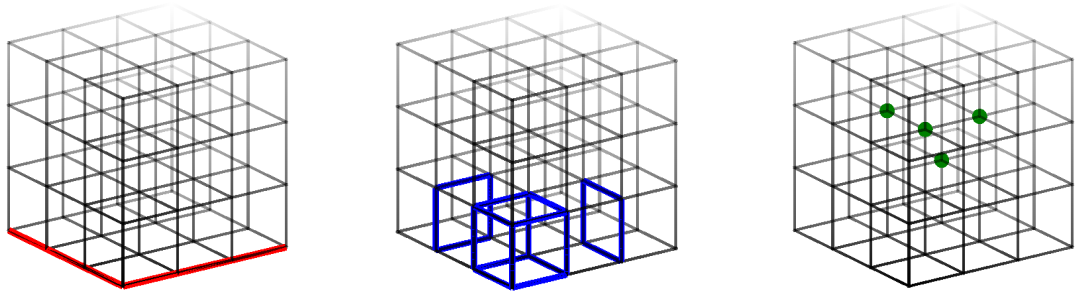

(a) irregular edges (b) $\breve{\mathbf{x}}^s_{A\cup A_\gamma}$ (c) $\breve{\mathbf{x}}^s_\Gamma$

Figure 4: BB-coefficient neighborhoods of a single box H^s: the expansion $\breve{\mathbf{x}}$ consists of terms up to order 2 in tri-cubic BB-form.

Example: For $m = 3$, let $\mathbf{0} := (0, 0, 0)$ be the index of the irregular point, the edge-indices $(\gamma, 0, 0)$ and $(0, \gamma, 0)$ be irregular and $(0, 0, \delta)$ regular, see Fig. 4a. Then at the irregular point, see Fig. 4,

$$A = \{(0,0,0),(0,1,0),(0,0,1),(0,1,1),(1,0,0),(1,1,0),(1,0,1),(1,1,1)\},$$
$$\Gamma = \{(2,2,1),(2,1,2)\} \cup \{(2,2,1),(1,2,2)\} \cup \{(1,1,2)\}$$

Γ has only four distinct entries and $\breve{\mathbf{x}}^s$ is displayed on the full tri-cubic grid but only consists of terms up to degree 2 from the bottom front irregular point. For the irregular edge E_1

$$A_{2,1} = \{(2,0,0),(2,1,0),(2,0,1),(2,1,1)\}.$$

◇

3. Initialization of control points and of a C^0 tri-cubic spline complex

This section describes the default initialization of the control points $\mathbb{c}^s_\alpha$ of the splines over the box-complex, and the BB-points $\mathbb{b}^s_\alpha$ of the BB-form pieces of the spline. Treating the location and associated value(s) of each box vertex as a control point, we can interpret, where regular, the box-complex with values as a control mesh of a tri-cubic

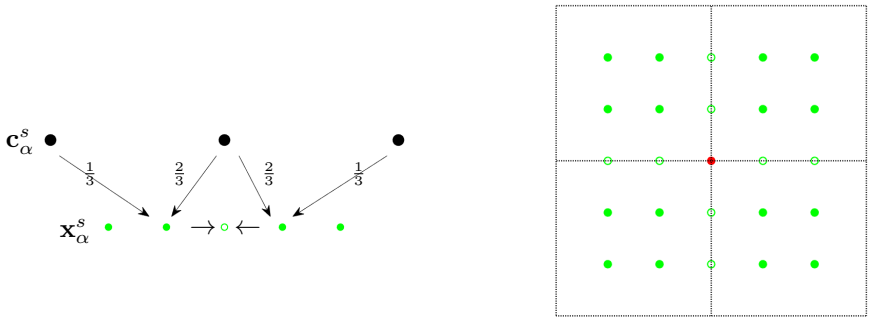

(a) $\circ = \frac{1}{2}\bullet + \frac{1}{2}\bullet = \frac{1}{6}\bullet + \frac{4}{6}\bullet + \frac{1}{6}\bullet$ (b) $\bullet = \frac{1}{2}\circ + \frac{1}{2}\circ$

Figure 5: Cubic C^2 B-spline control vertices $\bullet$ to BB-net $\mathbf{x}^s_\alpha$ conversion. The inner BB-coefficients $\bullet$ initialize the control abscissae $\mathbf{c}^s_\alpha$ of Fig. 1a.

C^2 spline in B-spline form with uniform knots (see de Boor (1978, 1987)). Expressing the spline pieces in BB-form, (by knot insertion, weighted averaging) is called *B-to-BB-conversion*. Fig. 5a depicts the formulas for converting the uniform degree three C^2 B-spline control points, marked as $\bullet$ (top), to BB-coefficients marked as $\bullet$ and $\circ$ (bottom). Fig. 5b illustrates the tensored version. The B-to-BB conversion can be broken into averaging steps, first initializing the inner 2^m BB-coefficients as uniform tri-linear averages of the vertices and then setting the inner BB-coefficients of faces, the edges and finally the vertex as the average of their index-wise nearest neighbors.

Initialization of the control points $\mathbb{c}^s_\alpha$ from the box-complex + data. For each box H^s with its 2^m vertices labeled j, locations $\mathbf{x}^s_j$ and data y^s_j, initialize $\mathbb{c}^s_\alpha := (\mathbf{x}^s_\alpha, y^s_\alpha) \in \mathbb{R}^{m+1}$, $1 \le \alpha_i \le 2$ by uniform tri-linear interpolation of the $(\mathbf{x}^s_j, y^s_j)$ (for $m = 2$ see the illustration to the right.)

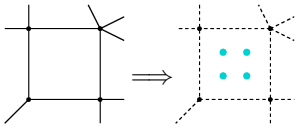

Definition 1. *The $\mathbb{c}^s_\alpha := (\mathbf{x}^s_\alpha, y^s_\alpha) \in \mathbb{R}^{m+1}$, $1 \le \alpha_i \le 2$ are called control points, the $\mathbb{b}^s_\alpha := (\mathbf{x}^s_\alpha, y^s_\alpha) \in \mathbb{R}^{m+1}$, $0 \le \alpha_i \le 3$ are called BB-points.*

3.1. The operator $\mathbf{S}$*:* $\mathbb{c}^s_\alpha \to \mathbb{b}^s_\alpha$

The operator consists of two steps: an averaging step that generalizes B-to-BB-conversion and – only if the box is irregular – a binary split to isolate singularities.

(i) Set inner box, inner face, inner edge and corner BB-points $\mathbb{b}^s_\alpha$, $0 \le \alpha_i \le 3$: for $1 \le \alpha_i \le 2$, $\mathbb{b}^s_\alpha := \mathbb{c}^s_\alpha$; for $d = 2$ down to $d = 0$, for each d-box Q shared by n_Q $d+1$-dimensional boxes $H^1, \dots, H^{n_Q}$ do as follows. Re-arrange the domain axes so that the $\mathbb{b}^s_\alpha$ have indices $\alpha := (\gamma, e_0)$, $\gamma \in \{1,2\}^d$ where e_0 is the zero in $\mathbb{N}_0^{m-d}$. Average (for $m = 2$ see the illustration to the right)

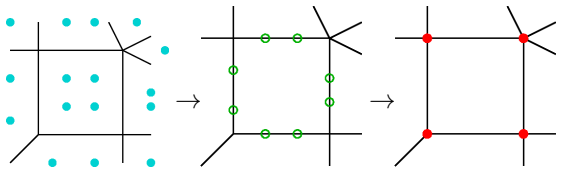

$$\mathbb{b}_{\gamma,e_0} := \sum_{s=1}^{n_Q} \mathbb{b}^s_{\gamma,e_1}/n_Q. \tag{2}$$

(ii) For each irregular box, re-represent its tri-cubic on each eighth of the domain by evenly subdividing (e.g. apply de Casteljau's algorithm to the BB-net at parameters $u = v = w = \frac{1}{2}$).

After Step (ii), we refer to the sub-boxes that contain the least-dimensional irregularity of the original box as *irregular sub-boxes*. For $m = 2$, i.e. for a bivariate mesh of quadrilaterals, Fig. 6 shows in color the BB-control polyhedra of three irregular sub-boxes.

Step (i) computes each BB-coefficient inner with respect to Q as the average of the closest BB-coefficients that are inner with respect to the boxes $H^1, \ldots, H^{n_Q}$ of one dimension higher. That is, for $d = 0$, $(\gamma, e_0) = (0, 0, 0)$ and $\mathbb{b}^s_{000}$ is initialized as the average of the index-wise nearest inner BB-coefficients of the edges emanating from $\mathbb{b}^s_{000}$. For $d = 1$, γ enumerates two coefficients $\mathbb{b}^s_{100}$ and $\mathbb{b}^s_{200}$ of an edge E, and each $\mathbb{b}^s_{\gamma 00}$ is initialized as the average of the inner BB-coefficients index-wise nearest to $\mathbb{b}^s_{\gamma 00}$ of the faces including the edge E. For $d = m - 1$, Eq. (2) is the *regular (univariate) C^1 constraint* (2'), i.e. the average of two BB-coefficients, one for each of the two boxes sharing the face.

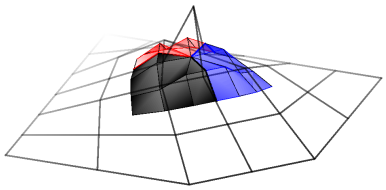

Figure 6: Illustration for $m = 2$: Initial and fine BB-net (with with bi-cubic BB-net interpolating facets colored) of the irregular sub-box for valence $n = 3$.

Example: For $d = 2$ and $m = 3$, consider adjacent boxes H^0, H^1 whose shared quad-face Q has 16 associated BB-coefficients $\mathbb{b}^0_{\gamma_1\gamma_2 0} = \mathbb{b}^1_{\gamma_1\gamma_2 0}$, $\gamma_i \in \{0, 1, 2, 3\}$. Then (2) simplifies to

$$\mathbb{b}^0_{\gamma_1\gamma_2 0} = \mathbb{b}^1_{\gamma_1\gamma_2 0} = (\mathbb{b}^0_{\gamma_1\gamma_2 1} + \mathbb{b}^1_{\gamma_1\gamma_2 1})/2 \qquad \text{for } 0 < \gamma_1, \gamma_2 < 3. \tag{2'}$$

For $d = 1$, the inner BB-coefficients $\mathbb{b}^s_{\gamma_1 00}$ on an edge surrounded by quads H^s, $s = 1, \ldots, n_Q$, are initialized to

$$\mathbb{b}^s_{100} = \sum_{k=1}^{n_Q} \mathbb{b}^s_{110}/n_Q, \quad \mathbb{b}^s_{200} = \sum_{k=1}^{n_Q} \mathbb{b}^s_{210}/n_Q \tag{3}$$

For $d = 0$, for a point $\mathbb{b}^s_{000}$ surrounded by boxes H^s, $s = 1, \ldots, n$,

$$\mathbb{b}^s_{000} = \sum_{k=1}^{n} \mathbb{b}^s_{100}/n \qquad \text{for } 0 < \gamma_1 < 3. \tag{4}$$

◇

3.2. *Interpretation and properties of* **S**

In the context of solving differential equations on a fixed manifold defined by $\mathbf{x}^s_\alpha$, the y^s_α serve as *degrees of freedom* associated with functions f^s_α (formally defined in Section 7).

Lemma 1 (C^2 where regular). *If the box H^s is regular then Initialization followed by the operator* **S** *gnerates a tri-cubic polynomial piece joined C^2 to its neighbors.*

Proof Since the vertices of a regular box are regular, any regular box provides the $2 \times 2 \times 2$ interior nodes of a regular $4 \times 4 \times 4$ grid that can be interpreted as C^2 tricubic B-spline control points. The claim follows since, for a regular box, **S** acts on the surrounding $4 \times 4 \times 4$ grid as B-to-BB conversion for an m-variate C^2 spline of degree 3 (whose control points are the grid points) de Boor (1987); Farin (2002). |||

Corollary 1. *The output of* **S** *is a spline complex of tensor-product degree* 3 *that is C^2 wherever boxes are regular and at least C^0 across irregularities.*

Moreover, the operator **S** converts any choice of $\mathbb{c}^s_\alpha$, not just $\mathbb{c}^s_\alpha$ generated by the default Initialization, into a C^1 spline in BB-form. Calling the $\mathbb{c}^s_\alpha$ control points is motivated by the following fact.

Observation 1. *The B-spline control points of a C^1 cubic spline coincide with the inner BB-coefficients of its pieces.*

We note that, while each Bernstein-Bézier basis function $B^3_{\alpha_1} B^3_{\alpha_2} B^3_{\alpha_3}$ associated with $\mathbb{b}^s_\alpha$ is restricted to one box, $\mathbb{c}^s_\alpha$ is associated with a smooth piecewise polynomial function supported on several boxes, as illustrated in Fig. 7. Observation 1 generalizes to the larger box-complex whereever a d-box is regular.

Corollary 2. *If a d-box H^s is regular then the operator* **S** *defines the BB-net of a C^1 d-cubic tensor-product spline.*

To ensure that the spline-complex controlled by the $\mathbb{c}^s_\alpha$ is everywhere at least C^1, not just where regular, the next section shows how to place the BB-coefficients with index in Γ into a linear subspace.

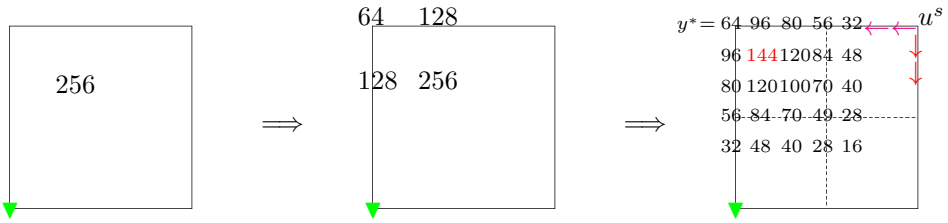

(a) control point $\mathbb{c}_{21}$ (b) BB-coefficients $\mathbb{b}_{ij}$ (c) split

Figure 7: Example $m = 2$. The only irregularity in the 2-box is marked as ▼. (Splitting of boxes guarantees that there is at most one irregular point per (sub-)box.) In the example, (a) the only control point with a non-zero value is $\mathbb{c}_{12} = (\mathbf{c}_{12}, y_{12})$ with Greville abscissa $\mathbf{c}_{12}$ and value $y_{12} = 2^8$. (b) The four non-zero y_α of $\mathbb{b}_\alpha$ for $\alpha \in \{02, 12, 03, 13\}$. (c) The non-zero BB-coefficients after splitting at $u = v = 0.5$. The parameter u^s will be used in the proof of Theorem 2 and the arrows hint at derivatives, e.g. $\partial^2_{-e_1} y(u^s) = 3 \cdot 2 \cdot 32 \neq 0$. Of the 2^2 bi-cubic maps surrounding and overlapping the corner marked by $y^* = 64$, only one has a non-zero inner coefficient index-wise nearest the corner (marked as 144) in the displayed polynomial piece.

4. Local linear expansion and composition (projection)

To enforce C^1 continuity, we derive for each irregularity a linear map that will be shared by the polynomial expansions joining at the irregularity. Since boxes containing an irregular point were split into 2^m sub-boxes, each resulting sub-box will have a most one singularity, and the linear maps (and constructions) at different irregular points will not interfere with one another.

4.1. A linear map ℓ

We determine a linear map ℓ that best fits the tangent data $y^s_\alpha, \alpha \in T$, at $\mathbf{x}^s_\alpha$.

One way to compute ℓ is as follows. For a local box-complex surrounding an irregular point, wlog. $\mathbf{x_0} = \mathbf{0}$, choose the four vertices $\Delta_0 := \sigma\,[-1, 1, 1]$, $\Delta_1 := \sigma\,[1, -1, 1]$, $\Delta_2 := \sigma\,[1, 1, -1]$, $\Delta_3 := \sigma\,[-1, -1, -1]$, of a regular simplex Δ to form the matrix

$$M := \begin{bmatrix} \Delta_0 & 1 \\ \Delta_1 & 1 \\ \Delta_2 & 1 \\ \Delta_3 & 1 \end{bmatrix} \in \mathbb{R}^{m+1,m+1}, \qquad \sigma := \sum_{s=1}^{n} \sum_{j=1}^{m} \frac{\|\mathbf{x}^s_\mathbf{0} - \mathbf{x}^s_{e_j}\|}{nm}. \tag{5}$$

The simplex provides a local coordinate system and helps to make the linear function concrete. Equi-distance of its vertices and scaling by σ aim to ensure numerical stability of the following fitting process (by proportionately covering the tangent neighborhood T); formally, the simplex shape and scaling do not affect volume or shape of the construction. The barycentric coordinates of $\mathbf{x}^s_\alpha$ with respect to Δ form the row vector

$$b^s_\alpha := [\mathbf{x}^s_\alpha, 1] M^{-1} \in \mathbb{R}^{m+1}. \tag{6}$$

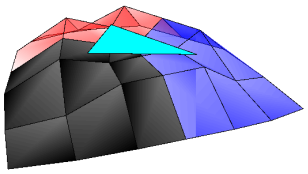

Figure 8: Illustration for $m = 2$ and valence $n = 3$. The central triangle represents the least-squares fit to the data and defines ℓ.

Denote by $b_T \in \mathbb{R}^{nm\times(m+1)}$ the matrix of barycentric coordinates $b^s_{e_j}$, $s = 1, \ldots, n$, $j = 1, \ldots, m$ and by $y_T \in \mathbb{R}^{nm}$ the column vector of associated data $y^s_{e_j}$. Then the column vector

$$\boldsymbol{\ell} := (b_T^\mathsf{t} b_T)^{-1} b_T^\mathsf{t} y_T \in \mathbb{R}^{m+1} \tag{7}$$

is the minimizer of $\min_{\boldsymbol{\ell}} \sum_{s=1}^{n} \sum_{\alpha\in T} \left(y^s_\alpha - b^s_\alpha \boldsymbol{\ell}\right)^2$. The values $\boldsymbol{\ell}_j$, $j = 0 \ldots m$ at the vertices Δ_j of Δ determine a linear map $\ell : \mathbb{R}^m \to \mathbb{R}$. For example, we can interpret $(\Delta_j, \boldsymbol{\ell}_j)$ as the abscissae and coefficients of a linear polynomial ℓ in *total degree* Bernstein-Bézier form (Farin, 2002, Chapter 17).

In the next section, we apply ℓ to the expansion $\breve{\mathbf{x}}$ by computing the barycentric coordinate vectors $\breve{b}^s_\alpha$ of the coefficients $\breve{\mathbf{x}}^s_\alpha$ of $\breve{\mathbf{x}}$ and setting $y^s_\alpha := \breve{b}^s_\alpha \boldsymbol{\ell} \in \mathbb{R}$, for $\alpha \in G$. Then the BB-coefficients $(\breve{\mathbf{x}}^s_\alpha, y^s_\alpha)$ will define abscissae and ordinates of the expansion ℓ^s in tensor-product BB-form of ℓ in sector s, i.e. in the box H^s.

Example: Continuing the previous bivariate example with y^s_α the third coordinate, we compute the best linear approximation in the form of a function over a 2-simplex. That is, we determine $\boldsymbol{\ell} \in \mathbb{R}^3$ at the vertices of a triangle (see Fig. 8). Fig. 9 shows the initial BB-coefficients (vertices of thin lines) and their projection onto ℓ^s (vertices of thick lines in the plane). ◇

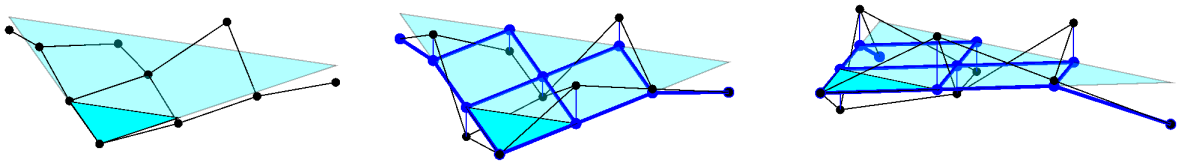

(a) partial BB-net with coefficients • and ℓ^s (b) two views of the input BB-net and projection $\ell^s(\mathbf{x}^s)$

Figure 9: Illustration for $m = 2$. Mapping the partial BB-net (of BB-coefficients • with index in $A \cup \Gamma$) of an m-cubic onto a sector ℓ^s of the linear map ℓ. The BB-coefficients in A will later be coalesced.

4.2. Projection along semi-regular edges

Let $\mathbb{b}_{\gamma 00}$ be the BB-coefficients associated with a semi-regular edge. We need only consider $\gamma \in \{1, 2\}$ since $\mathbb{b}_{000}$ and $\mathbb{b}_{300}$ will be set, in the last step of Algorithm C1 in Section 6, by regular C^1 constraints between the polynomial pieces of adjacent boxes. One option is to replicate the previous simplex-based construction for each fixed $\gamma \in \{1, 2\}$ and $m = 2$ as done for the illustrations in Fig. 8 and Fig. 9. Alternatively, we apply the following projection.

Planar projection P_n. The projection P_n applies to each coordinate k of $\mathbb{R}^{m+1}$ separately and to one (inner) index γ of one edge at a time. For fixed $ij \in \{00, 01, 10, 11, 12, 21\}$ and γ, after suitable re-arrangement of domain axes, denote by $c_{ij} := (c^s_{ij})_{s=1,\dots,n} \in \mathbb{R}^n$ the vector of the kth coordinate of the input BB-coefficients $\mathbb{b}^s_{\gamma ij}$; and by $x_{ab} := (x^s_{ab})_{s=1,\dots,n} \in \mathbb{R}^n$ the kth coordinate of the output BB-coefficients. We index so that $c^s_{20} = c^{s-1}_{02}$ (s is interpreted modulo n) and denote by $c^{\leftarrow}_{ij}$ the cyclic backward permutation of c_{ij} with respect to s and by $c^{\rightarrow}_{ij}$ the forward permutation. Then P_n maps the vectors c_{ij} to vectors x_{ab} with entries x^s_{ab} given by

$$x^s_{11} := x^s_{10} := x^s_{01} := x^s_{00} := \frac{1}{3n} \sum_{\sigma=1}^{n} c^\sigma_{11} + c^\sigma_{21} + c^\sigma_{12} \in \mathbb{R}, \quad s = 1, \dots, n, \tag{8}$$

$$\begin{aligned} x_{21} &:= x_{00} + \kappa Q_n \Big(2(c_{21} + c^{\leftarrow}_{12}) + c^{\rightarrow}_{21} + c_{12} \Big) \in \mathbb{R}^n, \quad Q_n := \Big(\cos \frac{2\pi(i-j)}{n} \Big)_{i=1..n, j=1..n} \in \mathbb{R}^{n \times n}, \\ x_{12} &:= x_{00} + \kappa Q_n \Big(c_{21} + c^{\leftarrow}_{12} + 2(c^{\rightarrow}_{21} + c_{12}) \Big) \in \mathbb{R}^n, \quad \kappa_{\text{default}} := \frac{\sqrt{2}}{4n \cos \frac{\pi}{n}}. \end{aligned} \tag{9}$$

Equation (8) coalesces the 1-neighborhoods of all sectors s into one central point and (9) places (the $m = 2$-dimensional projection neighborhood consisting of) $\breve{\mathbf{x}}^s_{\gamma 12}, \breve{\mathbf{x}}^s_{\gamma 21}$, $s = 1, \dots, n$, into a plane anchored at $\breve{\mathbf{x}}^s_{\gamma 00}$.

5. Singular reparameterization

Here we focus on the $\mathbf{x}$ coordinates of $\mathbb{b}^s_\alpha$ initialized by the operator $\mathbf{S}$ for an irregular sub-box. A *local box-complex surrounding* $\mathbf{p}$ consists of n boxes H^s, $s = 1, \dots, n$, that surround an irregular point $\mathbf{p}$ without gap and overlap. The *singular expansion* $\breve{\mathbf{x}}$ *at* $\mathbf{p}$ is defined by BB-coefficients $\breve{\mathbf{x}}^s_\alpha$, $\alpha \in G$, of the polynomial pieces $\breve{\mathbf{x}}^s$; $\breve{\mathbf{x}}^s$ corresponds to H^s and is singular at the common point $\breve{\mathbf{x}}^s_{000}$. Since boxes with one or more irregular points are split into 2^m (sub-)boxes, the singular expansions of irregular points will not interfere with one another.

The singular construction is motivated by the fact that, already for $m = 2$ and $n \neq 4$, parametric C^1 continuity and non-zero first derivatives imply loss of injectivity at the irregularity (Peters and Reif, 2008, Lemma 3.7). The basic idea is then to set the first derivatives to zero, and to have the second derivatives define a common tangent space that is parameterized with a singularity at the irregularity but can locally be equivalently represented by a regular smooth parametrization ℓ.

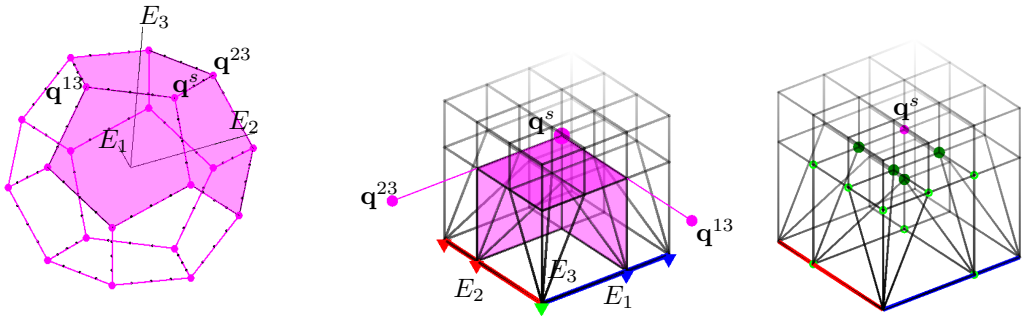

(a) intersection polyhedron (b) one box: intersecting planes (c) $\breve{\mathbf{x}}_\Gamma$ + C^1 averages ●

Figure 10: Intersection points $\mathbf{q}^s$. (a) Polyhedron with $n = 12$ facets, one for each edge E_k, $k = 1, \ldots, 12$. The irregular edges of one box are labeled E_1, E_2, E_3. (b) The BB-net of $\breve{\mathbf{x}}$ is shown completed to a tensor-product cubic. In the example the edges emanate from $\mathbf{0}$ at right angles and the $\mathbf{q}^{jk}$ are on a regular grid. The irregular point, marked ▼, is the superposition of all 2^m BB-coefficients in A. Two irregular edges have their coalesced BB-coefficients with index in A_γ marked ▼, respectively ▼. (c) The four BB-coefficients marked as larger, darker green ● form the $\breve{\mathbf{x}}_\Gamma$ and define the BB-coefficients of $\breve{\mathbf{x}}_{A_{\gamma,i}}$, marked by smaller, light green ●, by enforcing the regular univariate C^1 averaging constraints.

5.1. *Intersection polyhedron*

Central to the construction of the singular parameterization is a polyhedron that has one face for each edge E_k that emanates from the irregular point, see Fig. 10a. (The polyhedron is akin to the Voronoi diagram of the intersections of the E_k with a sphere enclosing the irregular point.) The polyhedron is spanned by n intersection points $\mathbf{q}^s$, one per box H^s. Each $\mathbf{q}^s$ is computed from m planes as follows. For each edge E_k, $k = 1, \ldots, m$ of H^s, let $H^1, \ldots, H^{n_k}$ be the boxes surrounding E_k. For fixed $j \neq k$, denote by $\mathbf{x}_{2e_k+e_j} \in \mathbb{R}^{n_k \times 3}$ the matrix with rows $\mathbf{x}^s_{2e_k+e_j}$, $s = 1, \ldots, n_k$, and by $\mathbf{x}_{2e_k} \in \mathbb{R}^{n_k \times 3}$ the matrix with repeated entries $\mathbf{x}^s_{2e_k}$. Then with Q_{n_k} defined by (9), the points

$$\mathbf{x}_{2e_k} + Q_{n_k}(\mathbf{x}_{2e_k+e_j} - \mathbf{x}_{2e_k}) \in \mathbb{R}^{n_k \times 3}$$

are co-planar and define a plane $\mathbb{P}_k$ anchored at $\mathbf{x}_{2e_k}$. Specifically, since Q_{n_k} is of rank 2, each plane $\mathbb{P}_k$ is spanned by the first two rows C_k of $Q_{n_k}(\mathbf{x}_{2e_k+e_j} - \mathbf{x}_{2e_k})$ and $\mathbf{x}^s_{2e_k}$. Therefore, for a pair of scalars μ_{ik}, μ_{jk} per k we have $\mathbf{q}^s = \mathbf{x}^s_{2e_k} - [\mu_{ik}, \mu_{jk}]C_k$ and $\mathbf{q}^s$ can be computed by solving the 9×9 system

$$[\mathbf{q}^s, \mu] \begin{bmatrix} I_3 & I_3 & I_3 \\ C_1 & \mathbf{0} & \mathbf{0} \\ \mathbf{0} & C_2 & \mathbf{0} \\ \mathbf{0} & \mathbf{0} & C_3 \end{bmatrix} = \left[\mathbf{x}^s_{2e_1}, \mathbf{x}^s_{2e_2}, \mathbf{x}^s_{2e_3}\right], \quad \mathbf{0} \in \mathbb{R}^{2\times m}, \mu \in \mathbb{R}^{2m}. \tag{10}$$

Since each $\mathbf{x}^s_{2e_k}$ is obtained by repeated averaging (B-to-BB conversion followed by de Casteljau's algorithm) that tend to equi-distribute points, solvability can be guaranteed under mild assumptions of non-degeneracy of the original box-complex.

An alternative construction of intersection points, that is simpler but less responsive to the $\mathbf{x}^s_\alpha$, is to translate so that $\mathbf{x}^s_{000} = \mathbf{0}$ and define the planes to be orthogonal to the $\mathbf{x}^s_{2e_i}$: $\mathbf{q}^s := [\nu_1, \nu_2, \nu_3][\mathbf{x}^s_{2e_1}, \mathbf{x}^s_{2e_2}, \mathbf{x}^s_{2e_3}]^{-\mathsf{t}}$, $\nu_i := \mathbf{x}^s_{2e_i} \cdot \mathbf{x}^s_{2e_i}$. (Well-formedness, Definition 2, guarantees the existence of the inverse matrix.)

5.2. *The BB-coefficients $\breve{\mathbf{x}}^s_\alpha$ of the singular parameterization*

The *expansion* $\breve{\mathbf{x}}^s$, at the irregular point $\breve{\mathbf{x}}^s_{\mathbf{0}}$ for box H^s, is represented by a collection of BB-coefficients $\breve{\mathbf{x}}^s_\alpha$ with index $\alpha \in G$. The expansion is defined as follows. Let E_i and E_k be two edges of H^s emanating from $\breve{\mathbf{x}}^s_{\mathbf{0}}$ (see Fig. 10). Denote as H^{ik} the box that shares with H^s the face spanned by E_i and E_k and as $\mathbf{q}^{ik}$ the intersection point of H^{ik}. Denote by n_k the number of boxes surrounding E_k (i.e. the edge E_k is regular iff $n_k = 4$). Then for $\alpha \in G$ and all $\{i, j, k\} = \{1, 2, 3\}$,

$$\breve{\mathbf{x}}^s_\alpha := \begin{cases} \breve{\mathbf{x}}^s_{\mathbf{0}} := \sum_{j=1}^{n} \mathbf{q}^j/n, & \text{if } \alpha_1, \alpha_2, \alpha_3 < 2; \\ \mathbf{x}^s_\alpha & \text{if } \alpha_k = 2, \alpha_i, \alpha_j \in \{0, 1\}; \text{ and } n_k = 4; \\ \breve{\mathbf{x}}^s_{2e_k} := \sum_{j=1}^{n_k} \mathbf{q}^{jk}/n_k, & \text{if } \alpha_k = 2, \alpha_i, \alpha_j \in \{0, 1\}; \text{ and } n_k \neq 4; \\ \mathbf{q}^s + \frac{2-\alpha_i}{4}(\mathbf{q}^{jk} - \mathbf{q}^s) & \text{if } \alpha_k = 2, \alpha_j = 2,\ \alpha_i \in \{0, 1\} \text{ and } n_k \neq 4. \end{cases} \tag{11}$$

Case 1 coalesces the coefficients of the trivariate 1-neighborhood A of $\breve{\mathbf{x}}^s_{\mathbf{0}}$. Case 2 simply copies the bivariate 1-neighborhood $A_{2,k}$ of $\mathbf{x}_{2e_k}$ to $\breve{\mathbf{x}}_{2e_k}$ if E_k is regular. If E_k is irregular, cases 3 and 4 establish a bivariate neighborhood of $\breve{\mathbf{x}}_{2e_k}$. Case 3 coalesces a bivariate 1-neighborhood of $\breve{\mathbf{x}}_{2e_k}$. Case 4 places BB-coefficients of the 2-ring about $\breve{\mathbf{x}}_{2e_k}$, e.g. 022 and 122, uniformly on (one half of) the line segment $\mathbf{q}^s$ to $\mathbf{q}^{jk}$ (shown purple in Fig. 10 and Fig. 12). Case 3 and 4 enforce a planarity constraint for a bivariate C^1 construction with locally removable singularity across irregular edges.

Example: Fig. 10b,c show $\breve{\mathbf{x}}^s$ when the edges emanating from $\mathbf{0}$ are at right angles and the relevant $\mathbf{q}^{jk}$ are on a regular grid. The second-order expansion $\breve{\mathbf{x}}^s$ is shown as part of a tri-cubic BB-net, for reference. Besides the irregular point there are two irregular edges (red, blue). The coalesced points indexed by A are represented by ▼. The coalesced points indexed by $A_{\gamma,1}$ are indicated by ▼, and $A_{\gamma,2}$ by ▼. The BB-coefficients marked as ● are determined by univariate C^1 constraints. Fig. 11 highlights the difference vectors of $\breve{\mathbf{x}}^s$ in Fig. 10b,c. The collection of red in Fig. 11 non-zero difference vectors in (a) are $\begin{bmatrix}0\\2\\0\end{bmatrix}^{\mathsf{t}}, \begin{bmatrix}0\\1\\0\end{bmatrix}^{\mathsf{t}}, \begin{bmatrix}0\\2\\1\end{bmatrix}^{\mathsf{t}}$. The green non-zero difference vectors in Fig. 11 are $\begin{bmatrix}0\\0\\2\end{bmatrix}^{\mathsf{t}}, \begin{bmatrix}0\\1\\2\end{bmatrix}^{\mathsf{t}}, \begin{bmatrix}1\\0\\2\end{bmatrix}^{\mathsf{t}}, \begin{bmatrix}1\\1\\2\end{bmatrix}^{\mathsf{t}}, \begin{bmatrix}0\\0\\1\end{bmatrix}^{\mathsf{t}}$ illustrating the separation of directional derivatives emphasized in Fig. 10c. ◇

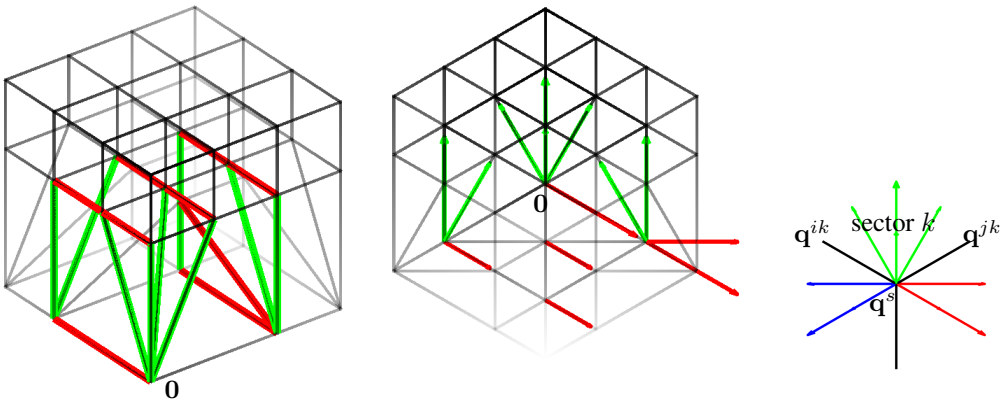

(a) BB differences (b) view of (c) from $e_i + e_j + e_k$ (c) differences in cones

Figure 11: Three views of the differences of the BB-coefficients near $\mathbf{0}$. (c) shows that the differences are zero or fall into separate cones.

Example: Fig. 12 illustrates the construction for $m = 2$ when the edges emanating from $\mathbf{0}$ are equally distributed in the plane. The point $\mathbf{q}$ of one sector of $\breve{\mathbf{x}}$ is the intersection of the lines dual to the edges. ◇

To prevent the BB-pieces from deviating too much from their box and so rule out overlap and degeneracy of the polynomial pieces associated with the boxes, from now on we require that the local box-complex surrounding an irregular point consists of boxes H^s that are sufficiently cube-like, defined as 'well-formed'.

Definition 2 (well-formed box-complex). *The local box-complex H^s, $s = 1, \ldots, n$, surrounding an irregular point is* well-formed *if for each s*

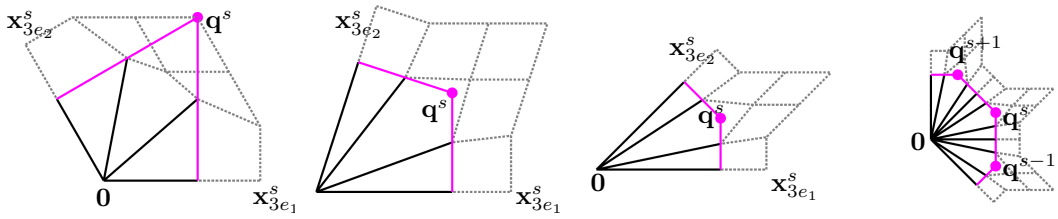

(a) $n = 3$ (b) $n = 5$ (c) $n = 8$ (d) $n = 8$, 3 sectors

Figure 12: $m = 2$: BB-net of a sector of a bivariate $\breve{\mathbf{x}}$ and equal angle $2\pi/n$. For context, dotted grey lines outline a possible completion to a bi-3 BB-net. (d) shows three sectors and the neighbor $\mathbf{q}^i$ across edge e_i The intersection point $\mathbf{q}^s$ is only used for the construction and is not part of the BB-net.

(a) the intersection $\mathbf{q}^s$ is well-defined (exists);
(b) $\breve{\mathbf{x}}^s_{2e_i}$, $i = 0, \dots, m$, form a coordinate system X^s that spans $\mathbb{R}^m$;
wlog. after shift $\breve{\mathbf{x}}^s_{2e_0} = \breve{\mathbf{x}}^s_{\mathbf{0}} = \mathbf{0}$ and we index so $\det(\breve{\mathbf{x}}^s_{2e_1}, \breve{\mathbf{x}}^s_{2e_2}, \breve{\mathbf{x}}^s_{2e_3}) > 0$.
(c) all coordinates of $\breve{\mathbf{x}}^s_\Gamma$ with respect to X^s are positive;
and, if E_k is regular then additionally the coordinates of $\breve{\mathbf{x}}^s_{2e_k+e_j}$, $j \neq k$, are non-negative.

Since the $\breve{\mathbf{x}}^s_{2e_i}$ are obtained from the vertices of the local box-complex by the uniform distribution (of the B-to-BB conversion) followed by repeated averaging (of the de Casteljau split at mid-points), well-formedness is not a severe imposition: the projection neighborhood is to lie in the cone of the $\breve{\mathbf{x}}^s_{2e_i}$, $i = 1, 2, 3$ with apex $\mathbf{0}$, and, for any regular edge E_k, the tangent neighbors of $\breve{\mathbf{x}}^s_{2e_k}$ with index $e_j + 2e_k$ lie in the same half space, anchored at $\breve{\mathbf{x}}^s_{2e_k}$, as does $\breve{\mathbf{x}}^s_{2e_j}$.

The following lemmas record facts about the construction that will help prove injectivity of the singular C^1 construction along an irregular edge.

Lemma 2. *Consider an irregular edge E_1 emanating from the irregular point $\breve{\mathbf{x}}^a_{000}$. Let H^a and H^b be two boxes of a well-formed box-complex and share a face including E_1 and another edge, E_2, emanating from $\breve{\mathbf{x}}^a_{000} = \breve{\mathbf{x}}^b_{000}$. Denote by $\breve{\mathbf{x}}^s$, $s \in \{a, b\}$ the corresponding expansions. Then*

(i) all $\breve{\mathbf{x}}^s_{2,\beta}$, $\beta_i \leq 2, \min\{\beta_i\} < 2$ lie in one plane.
(ii) $\breve{\mathbf{x}}^a$ and $\breve{\mathbf{x}}^b$ stay on opposite sides of their shared bivariate boundary defined by $\breve{\mathbf{x}}^a_{000} = \breve{\mathbf{x}}^b_{000}$, $\breve{\mathbf{x}}^a_{200} = \breve{\mathbf{x}}^b_{200}$, $\breve{\mathbf{x}}^a_{020} = \breve{\mathbf{x}}^b_{020}$, and $\breve{\mathbf{x}}^a_{220} = \breve{\mathbf{x}}^b_{220}$ (plus $\breve{\mathbf{x}}^a_{210} = \breve{\mathbf{x}}^b_{210}$ if E_2 is regular).
(iii) The derivatives of $\breve{\mathbf{x}}^a$ and $\breve{\mathbf{x}}^b$ across the shared face agree.

Proof Let H^s, $s = 1, \dots, n_1$, be the boxes that surround E_1. (i) By construction as intersections with the plane $\mathbb{P}_1$ of E_1, all $\mathbf{q}^s$ lie in $\mathbb{P}_1$ and, by (11), cases 3 and 4, so do all $\breve{\mathbf{x}}^s_{2,\beta}, \beta_i \leq 2, \min\{\beta_i\} < 2$. (ii) For a well-formed box-complex, the planar polygon formed by connecting the $\mathbf{q}^s$ in order does not cross itself since, by definition, boxes do not overlap. The $\breve{\mathbf{x}}^a_{22i}$, $\breve{\mathbf{x}}^b_{22i}$, $i = 0, 1$, are evenly distributed along the edges of the polygon and the regular C^1 constraint $\breve{\mathbf{x}}^a_{220} = \breve{\mathbf{x}}^b_{220} = (\breve{\mathbf{x}}^a_{221} + \breve{\mathbf{x}}^b_{221})/2$ holds. The bivariate 1-neighborhoods $\breve{\mathbf{x}}_{A_{2,i}}$, $i = 1, 2$ coalesce to the center of the planar polygon or satisfy regular C^1 constraints as averages of $\breve{\mathbf{x}}_{2e_i+2e_j+e_k}$. The remaining BB-coefficients coalesce at $\breve{\mathbf{x}}^a_{000}$. Therefore and by Definition 2(c), the two BB-nets each stay to one side of their shared $m-1$ dimensional boundary (whose BB-coefficients have subscripts $000, 200, 200, 220$ if E_2 is irregular or $000, 200, 200, 220, 210$ if E_2 is regular). (iii) Since the 1-neighborhoods $\breve{\mathbf{x}}_{A_{\gamma,i}}$ and $\breve{\mathbf{x}}_A$ are coalesced, the derivatives across the boundary are a multiple (shrinking to zero at the irregularities) of the non-zero C^1-matching differences $\breve{\mathbf{x}}^a_{221} - \breve{\mathbf{x}}^a_{220}$ and additionally, if E_2 is regular, of the C^1-matching differences $\breve{\mathbf{x}}^a_{121} - \breve{\mathbf{x}}^a_{120}$. |||

Lemma 3. *Except at the pre-images of irregularities the Jacobian determinant of $\breve{\mathbf{x}}^s$ is non-zero.*

Proof Without loss of generality, $\breve{\mathbf{x}}^s_{\mathbf{0}} = \mathbf{0}$. For easier reading of indices, we abbreviate the determinant of the $m \times m$ matrix

$$D(\nu_1 a, \nu_2 b, \nu_3 c) := \det(\breve{\mathbf{x}}^s_{\nu_1 e_a}; \breve{\mathbf{x}}^s_{\nu_2 e_b}; \breve{\mathbf{x}}^s_{\nu_3 e_c}).$$

For example, $D(2i, 2j, 2i + k) := \det(\breve{\mathbf{x}}^s_{2e_i}; \breve{\mathbf{x}}^s_{2e_j}; \breve{\mathbf{x}}^s_{2e_i+e_k})$. By well-formedness, and our sign convention $D_{222} := \det(\breve{\mathbf{x}}^s_{200}; \breve{\mathbf{x}}^s_{020}; \breve{\mathbf{x}}^s_{002}) > 0$. Then, by symbolic computation, the lowest-order terms of the Taylor expansion of the Jacobian determinant at $\mathbf{0}$ are

$$\begin{aligned}
&8u_1u_2u_3D_{222} + o(u_1u_2u_3) \\
&+ 4 \sum_{i:E_i \text{regular}} \sum_{j\in\{1,2,3\}\setminus i} u_i^3(u_jD(2i, 2j, 2i + k) + u_kD(2i, 2i + j, 2k)) + o(u_i^3(u_j + u_k)) \\
&+ 2 \sum_{i:E_i \text{regular}} \sum_{j\in\{1,2,3\}\setminus i} u_i^5D(2i, 2i + j, 2i + k) + o(u_i^5) \\
&+ 4 \sum_{i,j:E_i \text{ and } E_j \text{irregular}} u_i^3u_j^3D(2i, 2j, 2i + 2j + k) + o(u_i^3u_j^3).
\end{aligned} \tag{12}$$

Due to the ordering of the arguments, all expressions $D(\ldots)$ have the same sign as D_{222} and hence, apart from the pre-images of the irregularities, the determinant of the Jacobian is positive over the domain of $\breve{\mathbf{x}}^s$.

Now consider an irregular edge and a fixed γ. By Lemma 2 the BB-coefficients $\breve{\mathbf{x}}^s_{\gamma 21}$ and $\breve{\mathbf{x}}^s_{\gamma 12}$, $s = 1, \ldots, n_1$ lie in one plane. They also match the assumptions of Reif (1998); Nguyen and Peters (2016) to define a locally invertible C^1 *bivariate* expansion up to order 2 with an equivalent local regular parameterization (removable singularity) at the origin and non-zero Jacobian determinant apart from the origin. Since these expansions are tensored in the parameter along the irregular edge, the Jacobian only vanishes along the irregular edge. |||

Lemma 4. *For a well-formed box-complex, the leading principal minors of the Jacobian are positive.*

Proof Without loss of generality, we choose as the coordinate system $\breve{\mathbf{x}}^s_{2e_i} := e_i$, $i = 0, 1, 2, 3$. The first minor has the expansion

$$2u_1 + o(u_1) + \begin{cases} \breve{\mathbf{x}}^s_{122}(1)u_2^2u_3^2 + o(u_2^2u_3^2), & \text{if } E_i, i = 1, 2, 3, \text{irregular;} \\ \breve{\mathbf{x}}^s_{102}(1)u_3^2 + o(u_3^2), & \text{if } E_i, i = 1, 2, \text{irregular;} \\ \breve{\mathbf{x}}^s_{120}(1)u_2^2 + o(u_2^2) + \breve{\mathbf{x}}^s_{102}(1)u_3^2 + o(u_3^2), & \text{if } E_1 \text{ irregular or all } E_i \text{ are regular;} \end{cases} \tag{13}$$

where (1) indicates the first coordinate, which is positive by Definition 2(c). The second minor has the expansion

$$\begin{aligned}
&4u_1u_2 + o(u_1u_2) \\
&+ \begin{cases} \breve{\mathbf{x}}^s_{122}(1)u_2^3u_3^2 + \breve{\mathbf{x}}^s_{212}(2)u_1^3u_3^3 + o(u_2^3u_3^2, u_1^3u_3^3) & \text{if } E_i, i = 1, 2, 3, \text{irregular;} \\ 2\breve{\mathbf{x}}^s_{102}(1)u_3^2u_2 + 2\breve{\mathbf{x}}^s_{012}(2)u_1u_3^2 + o(u_3^2u_2, u_1u_3^2) & \text{if } E_i, i = 1, 2, \text{irregular;} \\ 2\breve{\mathbf{x}}^s_{102}(1)u_3^2u_2 + 2\breve{\mathbf{x}}^s_{012}(2)u_1u_3^2 + 2\breve{\mathbf{x}}^s_{120}(1)u_2^3 + o(u_3^2u_2, u_1u_3^2, u_2^3) & \text{if } E_i, i = 1, \text{irregular;} \\ 2\breve{\mathbf{x}}^s_{102}(1)u_3^2u_2 + 2\breve{\mathbf{x}}^s_{012}(2)u_1u_3^2 + 2\breve{\mathbf{x}}^s_{120}(1)u_2^3 + 2\breve{\mathbf{x}}^s_{210}(2)u_1^3 + o(\ldots) & \text{if } E_i \text{ are regular;} \end{cases}
\end{aligned} \tag{14}$$

which is also positive by Definition 2(c). The third minor is positive by Lemma 3 and the sign convention. |||

Lemma 5. *For a well-formed box-complex, the inverse $\breve{\mathbf{x}}^{-1}$ of $\breve{\mathbf{x}}$ is well-defined and continuous in a neighborhood of its irregularities.*

Proof By Lemma 2 the BB-nets of adjacent boxes stay confined within their separate curved cones. Therefore, $\breve{\mathbf{x}}^{-1}$ exists on the full neighborhood of $\breve{\mathbf{x}}^s_{\mathbf{0}} = \breve{\mathbf{x}}(\mathbf{0})$ if the each piece $\breve{\mathbf{x}}^s$, $s = 1, \ldots, n$, is injective in a neighborhood of $\mathbf{0} \in [0..1]^3$. After affine transformation, by well-formedness, we may assume $\mathbf{x}^s_{2e_k} = e_k$, $k = 1, 2, 3$. By Lemma 4, applying Sylvester's criterion, the Jacobian of $\breve{\mathbf{x}}^s$ is positive definite:

$$\text{for any row vector } \mathbf{v} \neq \mathbf{0} \in \mathbb{R}^m \text{ and } (u, v, w) \neq \mathbf{0}, \quad \mathbf{v}\nabla\breve{\mathbf{x}}^s(u, v, w)\mathbf{v}^\intercal > 0. \tag{15}$$

Assume $\breve{\mathbf{x}}^s$ is not injective. Then there exist $\mathbf{u}_0 \neq \mathbf{u}_1$ in U^s so that $\breve{\mathbf{x}}^s(\mathbf{u}_0) = \breve{\mathbf{x}}^s(\mathbf{u}_1)$. If we define $g(t) := (\mathbf{u}_1 - \mathbf{u}_0) \cdot \breve{\mathbf{x}}^s(\mathbf{u}_0 + t(\mathbf{u}_1 - \mathbf{u}_0))$ then $g(0) = g(1)$ and the mean value theorem implies that for $\mathbf{v} := \mathbf{u}_1 - \mathbf{u}_0$,

$g'(t) = \mathbf{v}\nabla\breve{\mathbf{x}}^s(\mathbf{u}_0 + t\mathbf{v})\mathbf{v}^\intercal$ vanishes for some $t \in (0..1)$. However, this contradicts positive definiteness of the Jacobian.

Since the irregular point bijectively maps to $\mathbf{0}$ and any irregular edge E_k parameterized by u bijectively maps to $\breve{\mathbf{x}}(ue_k)$, $\breve{\mathbf{x}}$ is injective and $\breve{\mathbf{x}}^{-1}$ is well-defined and continuous in a neighborhood of the irregularities. |||

Corollary 3. *$y := \ell \circ \breve{\mathbf{x}}$ admits the reparameterization $y(\breve{\mathbf{x}}^{-1}) = \ell$ near the origin.*

By Lemma 3 and inverse function theorem, $\breve{\mathbf{x}}$ is additionally bijectively C^1 apart from the irregularities.

6. Constructing the C^1 spline

The remaining task is to adjust, by an operator $\mathbf{P}$, the BB-nets of BB-coefficients $\tilde{\mathbb{b}}^s_\alpha \in \mathbb{R}^{m+1}$ of the irregular sub-boxes generated by $\mathbf{S}$ so that the ensemble has matching derivatives and, locally, an alternative regular C^1 parameterization.

Operator $\mathbf{P}$: $\tilde{\mathbb{b}}^s_\alpha \to \mathbb{b}^s_\alpha$
Input: $\tilde{\mathbb{b}}^s_\alpha$ of irregular sub-boxes H^s, $s = 1, \ldots, n$, surrounding and sharing an irregular point.
Output: C^1-adjusted $\mathbb{b}^s_\alpha$ of the irregular sub-boxes.

1. (ℓ) Determine M by (5) and $\boldsymbol{\ell}$ by (7).
2. ($\mathbf{q}^s$) For each irregular sub-box H^s compute the intersections $\mathbf{q}^s$ by (10).
3. ($\breve{\mathbf{x}}^s$) For each irregular sub-box H^s, compute the singular parameterization $\breve{\mathbf{x}}^s$ by (11).
   Issue a warning if the box-complex is not well-formed.
4. ($\mathbf{x}, y$) For each irregular sub-box H^s, for $\alpha \in G$,

$$\mathbf{x}^s_\alpha := \breve{\mathbf{x}}^s_\alpha, \qquad y^s_\alpha := \ell(\breve{\mathbf{x}}^s_\alpha) = \breve{b}^s_\alpha \boldsymbol{\ell} \in \mathbb{R}, \quad \text{where } \breve{b}^s_\alpha := [\breve{\mathbf{x}}^s_\alpha, 1]M^{-1}. \tag{16}$$

   For each semi-regular edge, apply P_n defined by (8) and (9), to set $(\mathbf{x}^s_\alpha, y^s_\alpha)$, $\alpha \in \Gamma_\gamma \cup A_\gamma$, $\gamma = 1, 2$.
5. (join irregular sub-boxes C^1) For every face with BB-coefficients $\mathbf{x}_{ij0}$ shared by an irregular sub-box H^a and a (regular or irregular) sub-box H^b, enforce regular C^1 continuity by averaging

$$\mathbb{b}^a_{ij0} = \mathbb{b}^b_{ij0} := (\mathbb{b}^a_{ij1} + \mathbb{b}^b_{ij1})/2. \tag{17}$$

Remark: No coefficients are averaged between any sub-box and neighboring regular full-sized box since these transition are already C^1 by $\mathbf{S}$.

Example: Fig. 13 illustrates the operator $\mathbf{P}$ for $m = 2$. BB-coefficients of Γ marked as disks • lie in one plane due to application of the projection P_5. The BB-coefficients marked as circles ○ are regular C^1 averages (17) of the disks, as are the BB-nets marked as ○ to guarantee a C^1 transition to the (gray-dashed) surrounding sub-box bi-cubic. ◇

Example: For $m = 2$, Fig. 14a illustrates an approximation of a quadrant of a disk where the irregular point is surrounded by $n = 3$ quadrilaterals. The value y_i at the irregular point is 1, the values at the other box-complex vertices are 0. Initialization and the operator $\mathbf{S}$ yield the three BB-nets in Fig. 14b. Each of the three sectors is split into four subpatches of degree bi-3. Only the bi-3 BB-net of the irregular sub-boxes are shown in Fig. 14c, enlarged in Fig. 14d where the best fitting 2-simplex (central triangle) is added. Fig. 14e,f show the resulting function and its iso-contours. ◇

Example: Fig. 15 illustrates the case $m = 3$. The four boxes model an octant of a solid ball (in Fig. 15a the red box is hidden). The octant has one 0-dimensional irregularity of valence $n = 4$ in the interior of the octant and four 1-dimensional irregularities of valence $n_1 = 3$. Each tri-cubic is split into 2^3 pieces. The refined pieces meeting at the irregular point are projected according to Step 4 of $\mathbf{P}$. Along the four irregular edges, each bivariate control net defines a bivariate C^1 expansion. Fig. 15b and c show smooth level sets and part of the BB-nets of the irregular sub-boxes. ◇

Let n_r be the number of regular boxes and n_i be the number of irregular boxes. Then the overall algorithm is summarized as follows.

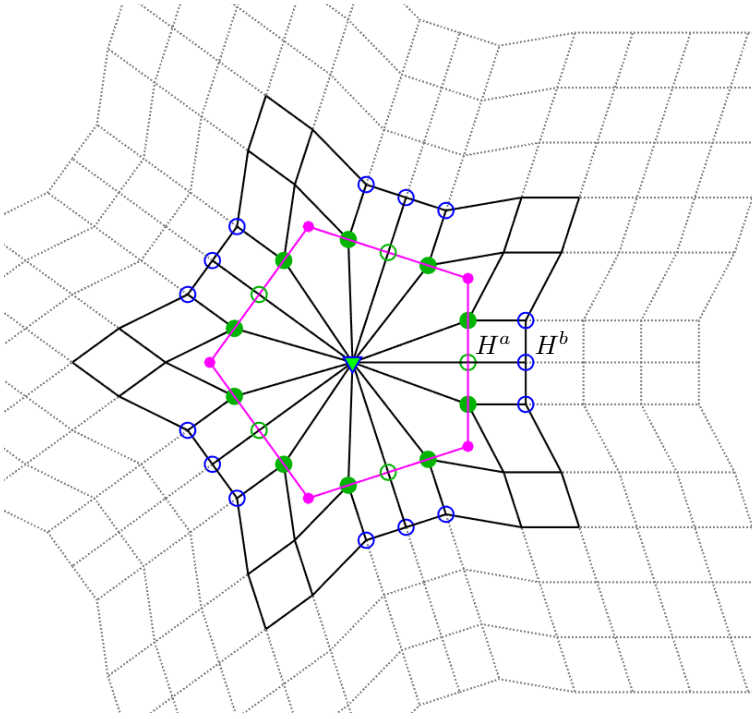

Figure 13: Illustration of $\mathbf{P}$ for $m = 2$ and five sectors. All $\mathbf{q}^s$, marked as •, are in the same plane and determine the BB-coefficients $\check{\mathbf{x}}_\Gamma$ marked as • and regular (univariate) C^1 constraints determine the BB-coefficients marked ○. The central point is the superposition of all BB-coefficients with indices in A. The last step of $\mathbf{P}$ sets the BB-coefficients marked ○ as averages to enforce regular C^1 constraints with the (first gray-dashed inner layer of the) outer sub-box neighbor of the irregular sub-box.

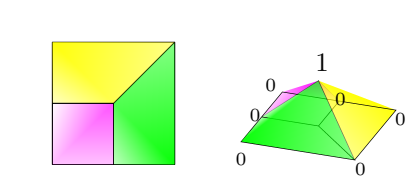

(a) input quads + data

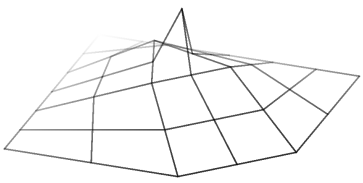

(b) initial BB-control net

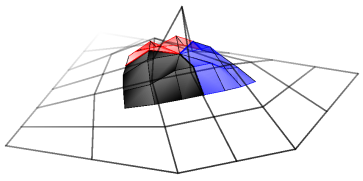

(c) initial + split net

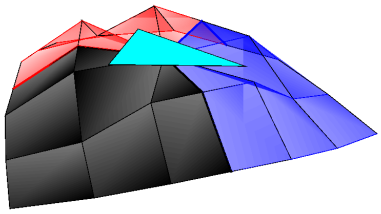

(d) split net + linear map

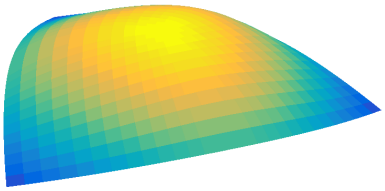

(e) BB-patch near irregularity

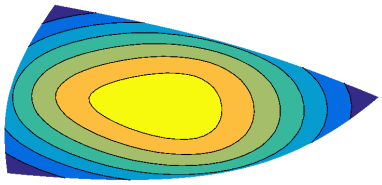

(f) Contour

Figure 14: Piecewise bi-3 C^1 quadrant of a disk with irregularity of valence $n = 3$ with non-zero value at the center (bi-linearly interpolated in (a) right).

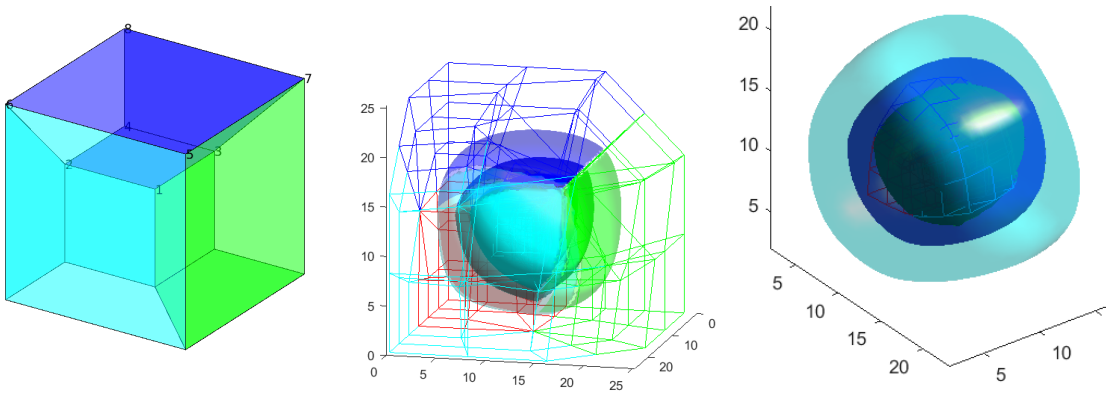

(a) local $n = 4$ box-complex (b) BB-net and level sets (c) nested level sets

Figure 15: C^1 approximation of the positive octant of a solid ball. The only non-zero datum is associated with the only interior vertex, the 0-dimensional irregularity shared by the 4 boxes (see (a)). (b) Four (color-coded) tri-3 BB-nets of the irregular sub-boxes. Note the coalesced BB-net along the four interior edges. (c) Three semi-transparent level sets of the function illustrate smoothness across singularities.

Algorithm C1.
Input: The vector $\mathbb{c}$ of $2^m(n_r + n_i)$ control points $\mathbb{c}^s_\alpha$ associated with the box-complex.
Output: The vector $\mathbb{b}$ of $4^m(n_r + 2^m n_i)$ BB-coefficients $\mathbb{b}^s_\alpha$ of a C^1 tri-cubic spline complex $(\mathbf{x}, y)$ over the box-complex.
With $\mathbf{P}$ acting only on irregular sub-boxes, $\mathbb{b} := \mathbf{PS}\mathbb{c}$.

7. Properties

For fixed outer boundaries, the dimension of the spline space over the box-complex with n boxes is $n2^m = 8n$. The singular spline space is C^1 with *removable singularities* in the sense that for any parameter where the spline has zero derivatives there locally exists an alternative non-singular C^1 expansion of the spline.

Theorem 1. *For a well-formed box-complex, the piecewise tri-cubic spline generated from the control points $\mathbb{c}^s_\alpha$ by Algorithm C1 is C^1 with removable singularities.*

Proof If all vertices of a box are regular, its vertices are interior to a $4 \times 4 \times 4$ grid of vertices. Initialization and $\mathbf{S}$ convert the grid into a tri-cubic tensor-product spline piece $[\mathbf{x}, y]$ in BB-form that is C^2-connected to its neighbors (Lemma 1). For irregular boxes, Steps 3 – 5 of $\mathbf{P}$ ensure that all derivatives of $[\mathbf{x}, y]$ across faces match, albeit with zero derivatives at irregularities; and, by Lemma 5, the inverse $\breve{\mathbf{x}}^{-1}$ of $\breve{\mathbf{x}}$ is well-defined and continuous in a neighborhood of any irregularity. Step 4 of $\mathbf{P}$ sets $y := \ell \circ \breve{\mathbf{x}}$ so that the expansion coefficients y_G are in the image of a linear map. Then $[\breve{\mathbf{x}}, \ell \circ \breve{\mathbf{x}}](\breve{\mathbf{x}}^{-1})$ is a local linear expansion of the function without singularity, i.e. the singularity is removable. At semi-regular edges, Step 4 places the lowest-order non-zero terms of the expansion at $\mathbf{x}_{\gamma 00}$ into a common linear subspace that satisfies the constraints for a removable singularity and bivariate C^1 continuity Reif (1997); Nguyen and Peters (2016). The placement in a plane of $\mathbf{x}_{2e_k+\beta_1 e_i+\beta_2 e_j}$, $\beta_i \leq 2$, $\beta \neq (2, 2)$ by Step 3 is consistent with this bivariate C^1 continuity. Since these bivariate C^1 expansions are tensored along the semi-regular edge, Step 5 completes the proof by joining with C^1 continuity any modified pieces to their neighbors on adjacent sub-boxes. |||

For $\alpha_i, \alpha'_i \in \{1, 2\}$, $i = 1, \ldots, m$, a C^1 generating function

$$f^s_\alpha : \mathbb{R}^m \to \mathbb{R},$$

is defined by setting $y^s_\alpha = 1$ and $y^{s'}_{\alpha'} = 0$ if either $\alpha' \neq \alpha$ or $s' \neq s$ (a different box) and applying Algorithm C1. Each function f^s_α is supported on several boxes H^k (cf. Fig. 7).

After one subdivision step applied to the box-complex (e.g. as in Burkhart et al. (2010)), each irregular box has at most one irregular point.

Theorem 2. *Consider a well-formed complex of boxes H^s with at most one irregular point per box. Then the generating functions f^s_α are linearly independent.*

Proof To show that we can restrict attention to the linear independence of the $n2^m$ generating functions of a local sub-complex of n boxes sharing and surrounding one irregular point of valence n, we select any *regular* point of the sub-complex and show that the 2^m generating functions f^s_α, $s = 1, \ldots, 2^m$, index-wise nearest to this regular point are linearly independent from one another. We choose the parameters and indices so that, for all s, $f^s_\alpha(0,0,0) = \mathbb{b}^s_{000}$ is the shared non-zero corner BB-coefficient, and define the functional $\mathcal{F}^r f := (\partial_{e_1}\partial_{e_2}\partial_{e_3} f\big|_{H^r})(0,0,0)$ that evaluates the mixed derivative of f restricted to the box H^r at the origin. Due to the de Casteljau split, the operator $\mathbf{P}$ at the irregular point does not reach the expansion up to degree two of f^s_α at $\mathbb{b}^s_{000}$ and, as for regular B-splines, $\mathcal{F}^r f^s_\alpha = 0$ unless $r = s$ (cf. Fig. 7c for $m = 2$). The functionals are therefore dual to the f^s_α, i.e. witness the linear independence of the f^s_α. The same functionals can be used to prove linear independence of the f^s_α at adjacent regular points. Since, by assumption, each irregular point is surrounded by regular vertices, in the remainder it suffices to consider one irregular point in isolation.

We focus on one irregular point surrounded and shared by a local sub-complex of n boxes H^s $s = 1, \ldots, n$ with $n2^3$ control points $\mathbb{c}^s_\alpha$. Let U^s be an s-labeled copy of $[0..2]^3$ and so that $[0..1]^3$ is the domain of the polynomial pieces associated with the irregular sub-boxes. We consider the functional

$$\mathcal{F}^s_\alpha f := \big(\prod_i \partial^{4-2\alpha_i}_{-e_i} f\big)(u^s), \quad u^s := (2,2,2) \in U^s$$

that, at the point u^s, evaluates mixed partial derivatives, of order 2 when $\alpha_i = 1$ and 0 when $\alpha_i = 2$, in reverse parameter directions (illustrated by arrows in Fig. 7c). It is easy to check that within the local sub-complex $\mathcal{F}^{s'}_{\alpha'} f^s_\alpha > 0$ when $s' = s$ and $\alpha' \le \alpha$, but $\mathcal{F}^{s'}_{\alpha'} f^s_\alpha = 0$ otherwise (cf. the non-zero coefficients in Fig. 7c).

Clearly $\mathcal{F}^{s'}_{222} f^s_\alpha = f^s_\alpha(2,2,2)$ is non-zero only for $s' = s$ and $\alpha = (2,2,2)$ showing that the f^s_{222} are linearly independent from each other and from all $n(2^3{-}1)$ f^s_α with $\alpha \neq (2,2,2)$. Therefore all f^s_{222} can be removed from consideration of linear dependence on H^s, $s = 1, \ldots, n$. Repeating this 'peeling away' argument, all f^s_α are removed in a descending order of the total sum $\alpha_1 + \alpha_2 + \alpha_3$. Finally, we observe that $\mathcal{F}^{s'}_{111} f^s_{111} = 0$ except when $s' = s$, i.e. also the f^s_{111} are linearly independent. For a box with one semi-regular edge (and no irregular point) the analogous argument for $m = 2$, for fixed $\gamma \in \{1, 2\}$, proves linear independence of the $f_{\gamma,\beta}$ from all other generating functions. |||

Remark. B-splines are not just linearly independent but locally linearly independent. No claim of *local* linear independence is made here, because too many f^s_α overlap near the irregular point. With more complex notation, a more general argument can apply the 'peeling away' approach to each maximal sub-complex of boxes with adjacent (non-isolated) irregular points.

Adaptive refinement and convergence estimates in engineering analysis require hierarchical refinement of the data function y associated with a fixed volumetric parameterization $\mathbf{x}$. To analyze hierarchical refinement of the space spanned by the f^s_α, the refinement operator can be restricted to the subset of nodes surrounding the irregular (extraordinary) point since the remainder is refined by uniform spline knot insertion (see e.g. Peters and Reif (2008)). So while the complete subdivision matrix has more rows (new refined nodes) than columns (old input nodes), for the operator it suffices to consider only a square sub-matrix that maps a fixed number of old nodes to the same number and layout of new nodes. Analogously, to characterize refinement of the space spanned by the f^s_α, only the mapping from a local complex of n irregular boxes surrounding an irregular point to n irregular sub-boxes is considered. Observation 1, that the B-spline control points of a C^1 cubic spline coincide with its inner BB-coefficients, motivates the following definition.

Definition 3 (Subdivision Operator $R\tilde{\mathbf{P}}\tilde{\mathbf{S}}$). *Given the vector $\mathbb{c}$ of control points $\mathbb{c}^s_\alpha$ of a local complex of n irregular boxes surrounding an irregular point, the vector $\tilde{\mathbb{c}}$ of refined control points $\tilde{\mathbb{c}}^s_\alpha$ of the complex of n irregular sub-boxes is $\tilde{\mathbb{c}} := R\tilde{\mathbf{P}}\tilde{\mathbf{S}}\,\mathbb{c}$. The connectivity follows from the 2^m-split of the boxes.*

- *The operator $\tilde{\mathbf{S}}$ equals $\mathbf{S}$ applied to the local complex with the output restricted to the n irregular sub-boxes.*
- *The operator $\tilde{\mathbf{P}}$ applies only to the y coordinate, and consists of Steps 4 and 5 of $\mathbf{P}$, with the collapsed $\breve{\mathbf{x}}_T$ replaced by the spanning $\breve{\mathbf{x}}_G$ in the definition (7) of $\boldsymbol{\ell}$:*

$$\boldsymbol{\ell} := (b_G^{\mathsf{t}} b_G)^{-1} b_G^{\mathsf{t}} y_G \in \mathbb{R}^{m+1}, \tag{7'}$$

  where $b_G \in \mathbb{R}^{ng\times(m+1)}$ is the vector of barycentric coordinates of ng coefficients $\breve{\mathbf{x}}_\alpha^s$, $\alpha \in G$, and $y_G \in \mathbb{R}^{ng}$ the data coordinate of $\mathbb{b}_\alpha^s$, $\alpha \in G$.
- *The operator R selects the inner BB-coefficients $\mathbb{b}_\alpha^s$, $1 \le \alpha_i \le 2$.*

Since the irregular structure (number of irregular points and irregular edges) is unchanged after applying $\tilde{\mathbf{S}}$, the operator $\tilde{\mathbf{P}}$ remains the same regardless of level of refinement. For example, $\tilde{\mathbf{P}}\tilde{\mathbf{S}}\tilde{\mathbf{S}}\mathbb{c}$ is well-defined.

Theorem 3. *The C^1 spline space of the data y on the fixed geometry $\mathbf{x}$ constructed by Algorithm C1 is refined by the subdivision operator $R\tilde{\mathbf{P}}\tilde{\mathbf{S}}$.*

Proof The operator $\tilde{\mathbf{S}}$ re-represents a spline on the n irregular sub-boxes surrounding an irregular point. The values y_α^s, $\alpha \in G$ have previously (in Step 4 of $\mathbf{P}$ or $\tilde{\mathbf{P}}$) been determined by a unique linear map ℓ. Therefore the least-squares fit (16) based on (7') re-creates ℓ, and $\tilde{\mathbf{P}}\tilde{\mathbf{S}} = \tilde{\mathbf{S}}$. The subdivision operator therefore re-represents y on the subdivided domain. |||

Remark. While splitting at the midpoint yields the standard convergence of the control net of y to the function y by a factor $1/4$, the radius of the tri-cubic pieces corresponding to the irregular sub-boxes does not halve but shrink by $3/8$. This is akin to many subdivision algorithms, except that subdivision contraction typically varies with n while the radius does not.

Lemma 6. *The splines constructed by Algorithm C1 reproduce linear functions.*

Proof Since tri-cubic splines reproduce polynomials of degree three, the claim holds where the box-complex is regular. Near irregularities, ℓ is the best fitting linear function to the linear data, hence reproduces the linear function, and (16) preserves linearity. |||

Due to the local support also pieces of linear functions can be reproduced.

The three theorems imply that the expressions $\sum_{s,\alpha} y_\alpha^s f_\alpha^s$ form a C^1 spline space over a box-complex. Regardless of regularity, the space offers 2^m uniformly distributed degrees of freedom y_α^s and is suitable, as has been verified, for finite element computations.

8. Discussion of Alternatives and Extensions

Fewer pieces. Since the goal of the splitting in $\mathbf{S}$ is to separate irregularities and so make $\mathbf{P}$ local, it is not necessary to split in directions where the spline space is a tensored space: if the box contains only semi-regular edges traced by the same parameter (parallel edges if the box is a cube) then there is no need to split along this parameter, see Fig. 16c. *Example:* Consider a box that contains only one semi-regular edge and no irregular point as in Fig. 2b. Such boxes need not be partitioned in the axial direction that tensors a bivariate (regular or irregular) mesh: the tri-cubic needs only be split into 2^2 pieces. ◇

Lower degree. Can we lower the degree of the C^1 tensor-product splines from cubic to quadratic? Due to coalescing BB-coefficients, quadratic boundary curves emanating from the irregular point become straight lines. This severely limits the polynomial reproduction of the space and is unacceptable for the shape of surfaces. Moreover, imposing smoothness leads to interdependence between the spline constructions at neighboring irregularities that may not be resolvable.

Higher Smoothness. In place of the linear map for C^k, $k = 1$, we can compose a unique Taylor expansion up to order $k+1$ with a k-fold coalesced, singular parameterization. In two variables, already Bohl and Reif (1997); Reif

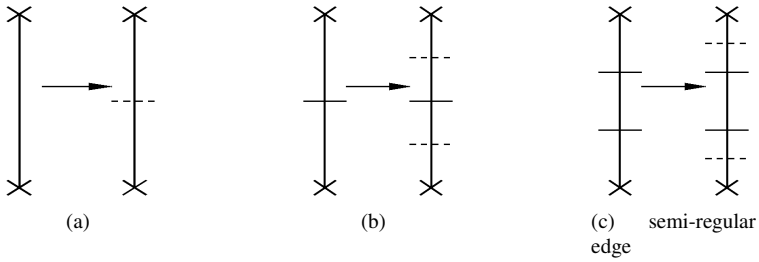

Figure 16: Three cases for Step (ii) of $\mathbf{S}$: (input mesh) $\rightarrow$ (split mesh). The $\times$'s at either end denote irregular points connected by a sequence of edges. The solid horizontal bars represent the original partition of the box-complex. The dashed bars indicate the partition due to splitting. (a,b) show required splits near the irregular points. (c) illustrates the case when no partition is needed for the middle semi-regular edge.

(1998) explored k-fold degeneracy using composition. Compared to that complete composition, replacing only the local expansion as in this paper can lower the polynomial degree.

Boundaries. A standard technique for modeling boundaries of manifolds is to virtually extend the original box-complex so that all original nodes are interior. One choice is to reflect the outermost boxes across their boundary faces and adjust for intersections and gaps; another is to replicate the boundary on top of itself to obtain an extension by zero-volume boxes. Algorithm C1 then applies to the original box-complex. To create a smooth the outer surface, the outermost layer of BB-coefficients can be replaced by those of a smooth bivariate construction, for example Nguyen and Peters (2016).

Higher number of variables. The concepts, constructions and proofs were set up to carry over to m-variate C^1 tensor-product splines for $m > 3$.

Adaptive C^1 spline spaces. In the bivariate case, e.g. PHT splines Kang et al. (2015) provide simple adaptive bi-cubic C^1 elements. We can apply the underlying principle: 'coarse determines fine wherever unrefined and refined splines meet' also to m-variate C^1 elements to obtain adaptive C^1 spline spaces.

Robustness. In the bivariate case, i.e. for unstructured quad meshes, the space tolerates extreme aspect ratios and even degeneration of the underlying box-complex, when used to solve higher-order differential equation in the Galerkin framework. The trivariate space may similarly be a good choice for *hex-dominant* constructions Owen (2001); Gao et al. (2017) that can include degenerate cells. An assessment of robustness and efficiency of the new trivariate space, based on an implemented solver for higher-order differential equations, is in progress.

Use as a manifold. If we define data $y^s_\alpha \in \mathbb{R}^k$, the construction yields a trivariate data manifold defined by $y : \mathbb{R}^3 \rightarrow \mathbb{R}^k$ in k-space. The bivariate free-form surface construction Nguyen and Peters (2016) can be interpreted as choosing $k = 3$ and defining $y : \mathbb{R}^2 \rightarrow \mathbb{R}^3$.

9. Conclusion

Tri-cubic splines represent an attractive combination of low polynomial degree, built-in smoothness and reproduction. This paper generalized C^1 tri-cubic splines to unstructured hex-meshes, guaranteeing smoothness also across irregular points and irregular edges. An explicit basis of 2^3 functions per hexahedral input box can reproduce linear functions, also locally, and is refinable. Data structures are not much more complex than those for tri-linear splines on hexahedral meshes and operations to evaluate position and derivatives are straightforward, based on the splines' tri-cubic Bernstein-Bézier pieces.

Acknowledgement. This work supported in part by DARPA TRADES and NIH EB018625.

Birner, K., Jüttler, B., Mantzaflaris, A., 2018. Bases and dimensions of C^1-smooth isogeometric splines on volumetric two-patch domains. Graphical Models 99, 46–56.

Bohl, H., Reif, U., 1997. Degenerate Bézier patches with continuous curvature. Computer Aided Geometric Design 14, 749–761.

de Boor, C., 1978. A Practical Guide to Splines. Springer.

de Boor, C., 1987. B-form basics, in: Farin, G. (Ed.), Geometric Modeling: Algorithms and New Trends, SIAM. pp. 131–148.

Burkhart, D., Hamann, B., Umlauf, G., 2010. Iso-geometric finite element analysis based on Catmull-Clark subdivision solids. Comput. Graph. Forum 29, 1575–1584.

Catmull, E., Clark, J., 1978. Recursively generated B-spline surfaces on arbitrary topological meshes. Computer-Aided Design 10, 350–355.
DeRose, T., 1990. Necessary and sufficient conditions for tangent plane continuity of Bézier surfaces. Computer Aided Geometric Design 7, 165–180.
Doo, D., Sabin, M., 1978. Behaviour of recursive division surfaces near extraordinary points. Computer-Aided Design 10, 356–360.
Eppstein, 1999. Linear complexity hexahedral mesh generation. CGTA: Computational Geometry: Theory and Applications 12.
Farin, G., 2002. Curves and Surfaces for Computer Aided Geometric Design: A Practical Guide. Academic Press, San Diego.
Gao, X., Jakob, W., Tarini, M., Panozzo, D., 2017. Robust hex-dominant mesh generation using field-guided polyhedral agglomeration. ACM Trans. Graph 36, 114:1–114:13. URL: http://doi.acm.org/10.1145/3072959.3073676.
Gregory, J.A., 1974. Smooth interpolation without twist constraints. Academic Press. pp. 71–88.
Gregson, J., Sheffer, A., Zhang, E., 2011. All-hex mesh generation via volumetric polycube deformation. Comput. Graph. Forum 30, 1407–1416.
Johnen, A., Weill, J.C., Remacle, J.F., 2017. Robust and efficient validation of the linear hexahedral element. Procedia Engineering, Elsevier, Itl. Meshing Roundtable , +1–13.
Kang, H., Xu, J., Chen, F., Deng, J., 2015. A new basis for PHT-splines. Graphical Models 82, 149–159.
Karčiauskas, K., Myles, A., Peters, J., 2006. A C^2 polar jet subdivision, in: Scheffer, A., Polthier, K. (Eds.), Proceedings of Symposium of Graphics Processing (SGP), June 26-28 2006, Cagliari, Italy, ACM Press. pp. 173–180.
Karčiauskas, K., Peters, J., 2016. Minimal bi-6 G^2 completion of bicubic spline surfaces. Computer Aided Geometric Design 41, 10–22.
Karčiauskas, K., Peters, J., 2017. Improved shape for refinable surfaces with singularly parameterized irregularities. Computer Aided Design 90, 191–198.
Karčiauskas, K., Peters, J., 2007. Bicubic polar subdivision. ACM Trans. Graph. 26, 14.
Liu, H., Zhang, P., Chien, E., Solomon, J., Bommes, D., 2018. Singularity-constrained octahedral fields for hexahedral meshing. ACM Trans. Graph 37, 93:1–93:17. URL: http://doi.acm.org/10.1145/3197517.3201344.
Loop, C.T., Schaefer, S., 2008. G ^{2} tensor product splines over extraordinary vertices. Comput. Graph. Forum 27, 1373–1382.
MacCracken, R., Joy, K.I., 1996. Free-form deformations with lattices of arbitrary topology, in: Proceedings of the ACM Conference on Computer Graphics, ACM, New York. pp. 181–188.
Meyers, R.J., Tautges, T.J., 1998. The "hex-tet" hex-dominant meshing algorithm as implemented in cubit, in: Freitag, L.A. (Ed.), Itl. Meshing Roundtable, pp. 151–158. URL: http://imr.sandia.gov/papers/imr7.html.
Mitchell, S.A., 1999. The all-hex geode-template for conforming a diced tetrahedral mesh to any diced hexahedral mesh. Eng. Comput. (Lond.) 15, 228–235.
Myles, A., Peters, J., 2009. Bi-3 C^2 polar subdivision. ACM Transactions on Graphics 28. Siggraph 2009.
Myles, A., Peters, J., 2011. C^2 splines covering polar configurations. Computer Aided Design 43, 1322–1329.
Neamtu, M., Pfluger, P.R., 1994. Degenerate polynomial patches of degree 4 and 5 used for geometrically smooth interpolation in 3. Computer Aided Geometric Design 11, 451–474.
Nguyen, T., Peters, J., 2016. Refinable C^1 spline elements for irregular quad layout. Computer Aided Geometric Design 43, 123–130.
Nieser, M., Reitebuch, U., Polthier, K., 2011. Section 2: CUBE COVER — parameterization of 3D volumes. Computer Graphics Forum 30, 1397–1406.
Owen, S.J., 2001. Hex-dominant mesh generation using 3d constrained triangulation. Computer-Aided Design 33, 211–220.
Owen, S.J., Brown, J.A., Ernst, C.D., Lim, H., Long, K.N., 2017. Hexahedral mesh generation for computational materials modeling. Procedia Engineering, Elsevier, Itl. Meshing Roundtable , +1–13.
Peters, J., 1991a. Parametrizing singularly to enclose vertices by a smooth parametric surface, in: MacKay, S., Kidd, E.M. (Eds.), Graphics Interface '91, Calgary, Alberta, 3–7 June 1991: proceedings, Canadian Information Processing Society. pp. 1–7.
Peters, J., 1991b. Smooth interpolation of a mesh of curves. Constructive Approximation 7, 221–247.
Peters, J., 2002. Geometric continuity, in: Handbook of Computer Aided Geometric Design, Elsevier. pp. 193–229.
Peters, J., Reif, U., 2008. Subdivision Surfaces. volume 3 of *Geometry and Computing*. Springer-Verlag, New York.
Pfluger, P.R., Neamtu, M., 1993. On degenerate surface patches. Numerical Algorithms 5, 569–575.
Prautzsch, H., Boehm, W., Paluszny, M., 2002. Bézier and B-spline techniques. Springer Verlag.
Reif, U., 1997. A refinable space of smooth spline surfaces of arbitrary topological genus. Journal of Approximation Theory 90, 174–199.
Reif, U., 1998. TURBS—topologically unrestricted rational B-splines. Constructive Approximation 14, 57–77.
Shi, K.L., Yong, J.H., Tang, L., Sun, J.G., Paul, J.C., 2013. Polar nurbs surface with curvature continuity. Comput. Graph. Forum 32, 363–370.
Toshniwal, D., Speleers, H., Hiemstra, R.R., Hughes, T.J., 2017a. Multi-degree smooth polar splines: A framework for geometric modeling and isogeometric analysis. Computer Methods in Applied Mechanics and Engineering 316, 1005 – 1061. URL: http://www.sciencedirect.com/science/article/pii/S004578251631533X, doi:https://doi.org/10.1016/j.cma.2016.11.009. special Issue on Isogeometric Analysis: Progress and Challenges.
Toshniwal, D., Speleers, H., Hughes, T.J., 2017b. Smooth cubic spline spaces on unstructured quadrilateral meshes with particular emphasis on extraordinary points: Geometric design and isogeometric analysis considerations. Computer Methods in Applied Mechanics and Engineering , 411–458.
Walfisch, D., Ryan, J.K., Kirby, R.M., Haimes, R., 2009. One-sided smoothness-increasing accuracy-conserving filtering for enhanced streamline integration through discontinuous fields. J. Sci. Comput 38, 164–184.
Warren, J.D., 1992. Creating multisided rational Bézier surfaces using base points. ACM Trans. Graph 11, 127–139. URL: http://doi.acm.org/10.1145/130826.130828.
Wei, X., Zhang, Y.J., Toshniwal, D., Speleers, H., Li, X., Manni, C., Evans, J.A., Hughes, T.J., 2018. Blended b-spline construction on unstructured quadrilateral and hexahedral meshes with optimal convergence rates in isogeometric analysis. Computer Methods in Applied Mechanics and Engineering 341, 609 – 639. URL: http://www.sciencedirect.com/science/article/pii/S004578251830344X, doi:https://doi.org/10.1016/j.cma.2018.07.013.
Yamakawa, S., Shimada, K., 2002. Hexhoop: Modular templates for converting a hex-dominant mesh to an all-hex mesh. Eng. Comput. (Lond.) 18, 211–228.